PU/NE-03-11

U. S. Department of Energy
Nuclear Engineering Education Research

INCIPIENT TRANSIENT DETECTION IN REACTOR SYSTEMS: EXPERIMENTAL AND THEORETICAL INVESTIGATION

Project Carried Out With Support From US DOE Under

Award NO: DE-FG07-02ID14339

Yearly Report
(June 1, 2002 to August, 2003)

S. T. Revankar, L. H. Tsoukalas, and R. Sattuluri

SCHOOL OF NUCLEAR ENGINEERING

U. S. Department of Energy
Nuclear Engineering Education Research

INCIPIENT TRANSIENT DETECTION IN REACTOR SYSTEMS: EXPERIMENTAL AND THEORETICAL INVESTIGATION

Yearly Progress Report
July 1, 2002 to September, 2003

Contributing Authors:

S. T. Revankar, L. H. Tsoukalas, and R. Sattuluri

Purdue University
School of Nuclear Engineering
West Lafayette, IN 47906-1290

Contact: Dr. Shripad T. Revankar
School of Nuclear Engineering
Purdue University
West Lafayette, In 47907-1290

765-496-1782
shripad@ecn.purdue.edu

October 2003

CONTENTS

LIST OF FIGURES v

LIST OF TABLES vii

ACRONYMS vii

NOMENCLATURE viii

EXECUTIVE SUMMARY x

1. INTRODUCTION 1
   1.1 Statement of the Problem 1
   1.2 Significance of the Problem 1
   1.3 References 2

2. OBJECTIVES AND TASKS 3
   2.1 Objectives 3
   2.2 Tasks 3

3. PROTREN METHODOLOGY
   3.1 PROTREN Description 4
   3.2 References 9

4. THEORETICAL SIMULATION OF TWO PHASE FLOW 10
   4.1 Simulation of Bubbly Flow 11
   4.2 Simulation of Slug Flow 15
   4.3 Simulation of Churn Flow 19
   4.4 Simulation of Annular Misty Flow 21

4.5 SPRT for On-Line Diagnosis of Flow Pattern Recognition. 28
4.5.1 SPRT Method 28
4.5.2 Test Approach 29
4.5.3 Test Results 30
4.5.3.1 Comparison between two SPRT methods 30
4.5.3.2 Parametric study of SPRT for flow pattern transition 31
4.6 References 44

5. EXPERIMENTAL PROGRAM 46
5.1 Experimental Loop 46
5.2 Experimental Data 51

6. PROTREN RESULTS 53

7. SUMMARY OF THE FIRST YEAR WORK 57

8. FUTURE WORK 58

LIST OF FIGURES

Figure 3.1. Flowchart of the fuzzy methodology 4

Figure 3.2 PROTREN results for a decreasing signal trend 7

Figure 3.3 PROTREN results for an unchanging signal trend 8

Figure 4.1.Bubbly Flow Simulation Geometry 11

Figure 4.2. Idealized output voltage of conductivity probe 12

Figure 4.3 Schematic of spherical bubble and conductivity probe 12

Fig4.4 Signal time traces for Bubbly Flow 13

Fig4.5. Void fraction time traces for Bubbly Flow 13

Fig.4.6. PDF of void fraction for Bubbly Flow 14

Fig.4.7. PDF of transition time for Bubbly Flow 14

Fig.4.8. Signal time traces for Slug Flow 17

Fig.4.9. Void fraction time traces for Slug Flow 17

Fig.4.10. PDF of Void fraction for Slug Flow 18

Fig.4.11. PDF of transition time for Slug Flow 18

Fig.4.12. Signal time traces for Churn Flow 23

Fig.4.13. Void fraction time traces for Churn Flow 23

Fig.4.14. PDF of Void fraction for Churn Flow 24

Fig.4.15. PDF of transition time for Churn Flow 24

Fig.4.16. Signal time traces for Annular-Misty Flow 26

Fig.4.17. Void fraction time traces for Annular-Misty Flow 26

Fig.4.18. PDF of Void fraction for Annular-Misty Flow 27

Fig.4.19. PDF of transition time for Annular-Misty Flow 27

Fig. 4.20. Comparison of two SPRT methods for the transition between bubbly and slug flow 33

Fig. 4.21 Comparison of two SPRT methods for the transition between bubbly, cap and slug flow 33

Fig. 4.22. Comparison of two SPRT methods for the transition between bubbly and slug flow. 34

Fig. 4.22. Comparison of two SPRT methods for the transition between bubbly and slug flow. 34
Fig. 4.23 Detection of change of gas/liquid flow rate in bubbly flow using average SPRT. 35
Fig. 4.24 Detection of change of gas/liquid flow rate in bubbly flow using SPRT based on average transition time. 35
Fig. 4.25 Detection of change of gas/liquid flow rate in bubbly flow using average SPRT. 36
Fig. 4.26 Detection of change of gas/liquid flow rate in bubbly flow using average SPRT. 36
Fig. 4.27 Detection of change of gas/liquid flow rate in bubbly flow using SPRT based on average transition time. 37
Fig 4.29 Slug and churn flow transition using SPRT based on average transition time. 37
Fig 4.30 Slug and churn flow transition using average SPRT. 38
Fig 4.31 Slug and churn flow transition using SPRT based on average transition time. 38
Fig 4.32 Slug and churn flow transition using average SPRT. 39
Fig 4.33 Slug and churn flow transition using SPRT based on average transition time. 39
Fig 4.34 Slug and churn flow transition using average SPRT. 40
Fig 4.35 Transition between bubbly, cap and slug flow using SPRT based on average transient time for different cap sizes. 40
Fig 4.36 Transition between bubbly, cap and slug flow using average SPRT for different cap sizes. 41
Fig 4.37 Transition between bubbly, cap and slug flow using SPRT based on average transient time for different cap frequencies. 41
Fig 4.38 Transition between bubbly, cap and slug flow using average SPRT for different cap sizes. 42
Fig 4.39 Transition between bubbly, cap and slug flow using SPRT based on average transient time for different thresholds. 42

Fig 4.40 Transition between bubbly, cap and slug flow using average SPRT for different thresholds. 43
Fig. 5.1. Inlet to the test section 46
Fig. 5.2. Schematic of the experimental loop 48
Fig. 5.3 Schematic of the comparator Circuit 52
Fig 5.4 Sample output from the data acquisition system 52
Fig. 6.1 actual data and normalized data for an increasing transient 54
Fig. 6.2 PROTREN result for an increasing transient 54
Fig. 6.3 Actual and Normalized data for fluctuating transient 55
Fig. 6.4 PROTREN result for a fluctuating transient. 55
Fig. 6.5 Actual and normalized data for a decreasing transient 56
Fig. 6.6PROTREN result for a decreasing transient. 56

LIST OF TABLES

Table 5.1 List of Instruments 49

ACRONYMS

PROTREN	Fuzzy methodology program for incipient detection of transient
SPRT	Sequential Probability Ratio Testing
PUMA	Purdue University Multi-Dimensional Test Assembly

NOMENCLATURE

Symbols

D – diameter

d – diameter

E_d – Entrainment rate.

g – gravitational constant

H – Hypotheses

j – total superficial velocity

L – Length

m – mean

n – average sample number

N_μ – viscosity number

r – radius

Re – Reynolds Number

T – Time;

v – velocity

V – velocity

Z – SPRT value

Greek Symbols

α – Void fraction, error probability

β – error probability

σ – surface tension

Δ – differential

ρ – mass density

γ – kinematic viscosity

θ – arbitrary parameter

μ – Viscosity

ξ – random number between 0 and 1

Subscripts

* - non dimensional quantity

b – bubble

E – entrance

f – fluid

g – gas

i – number

m – median

n – number

p – power

s – slug

v – volume

TB – Taylor Bubble

max – maximum

min – minimum

EXECUTIVE SUMMARY

The main goal of this research is to develop a method for detecting reactor system transients at the earliest possible time through a comprehensive experimental, testing and benchmarking program. This approach holds strong promise for developing new diagnostic technologies that are non-intrusive, generic and highly portable across different systems. It will help in the design of new generation nuclear power reactors which utilize passive safety systems with a reliable and non-intrusive multiphase flow diagnostic system to monitor the function of the passive safety systems. The objectives of the three year research project are: 1) Substantially improve PROTREN to include more features such as higher order statistical moments, SPRT (Sequentially Probability Ratio Testing) decision and Bayesian inference. 2) Develop separate effects experimental testing program and validate PROTREN using dynamic test data. 3) Develop heat transfer experimental program and benchmark PROTREN transient detection method. 4) Develop integral system testing of PROTREN using a scaled advanced boiling water reactor system and a small university nuclear reactor neutron flux data. 5) Develop prototype application of the PROTREN to detect incipient of transient.

The present three years research program is structured around three phases:

Phase 1: (July 1, 2002 to June 30, 2003) The work during phase 1 will concentrate on developing the PROTREN methodology by including additional features and enhancing the reliability of PROTREN's output. The following tasks are performed under this phase: Task1: Identification of Multiple Transients. Task 2: More efficient detection features. Task 3: PROTREN with Non-Gaussian noise and Task 4: Trade offs between Conservative and Active Detection.

Phase 2: This phase will last for the next 12 months. During this period of time, we will begin to apply the methodology developed during Phase 1 to simple experimental systems. The validation of the new PROTREN is carried out using 1) a simulated signal, 2) dynamic data from an experimental loop and 3) comparison of the PROTREN performance with the Sequential Probability Ratio Test (SPRT). The benchmarking of the PROTREN is carried out using the dynamic data from an experimental loop on the tube condensation. These result in the following tasks: Task 5: Simulated signal testing. Task 6: Experimental data testing. Task 7: Systematic comparisons and validation and Task 8 Benchmarking with heat transfer data.

Phase3: This phase, which will also last for 12 months, has two main tasks. The first one is the testing of PROTREN with neutron flux data in a small nuclear reactor. Task 9 involves an integral facility transient testing. This is done on a scaled integral test loop called PUMA (Purdue University Multi-Dimensional Test Assembly). For Task 10, Nuclear reactor neutron flux data testing, sub-critical multiplication tests are carried out on the PUR-1. This involves step change of the reactivity by pulling out control rods. The signals from the reactor are used in the testing of PROTREN for any incipient change during the criticality experiments that are conducted on this facility.

1. INTRODUCTION

1.1 Statement of the Problem

Often, non-operational reactor system transients are slow to develop and mature to a level challenging safety and control systems. Typically a very short-lived indication appears which if reliably identified shows that a component such as a valve, a motor, or a pump or an entire system such as Chemical and Volume Control System (CVCS) may be undergoing a significant change of state. Unfortunately, the indication quickly disappears due to the fact that seconds or minutes later (depending on the inertias of the variables involved) various controllers respond and in doing so obliterate evidence for an emerging transient. It is possible then that although everything appears to be normal, hours, days, or even months later there appears a major transient, called "unanticipated," in the sense that the original cause was never detected, which may have adverse operational and safety consequences. The proposed research is aimed at developing a methodology for detecting such "unanticipated" transients at the earliest possible time.

1.2 Significance of the Problem

Transient detection is an important part of computer-based monitoring, diagnostic and control systems. Stated simply, the main problem is to detect the onset of a meaningful departure from steady state and the direction of change, that is, whether the departure is in an increasing or decreasing direction. This is an essential first for reliable and timely diagnostics. Although conventional detection methods have been extensively studied and widely applied to this problem, they are generally signal and process dependent, and hence, cannot be easily ported to other processes and plants without further development. In addition, sufficiently large time windows are generally needed in conventional methods, which is not desirable for on-line signal transient detection and identification. The desired methodology should be signal and process independent, with a relatively small time, fast response, and high stability at the same time (Reifman, 1997). Argonne National Laboratory (ANL) and Purdue University have collaborated on the development of a novel operator advisory knowledge-based digital system called IGENPRO ((Mormam, 1997) (Reifman, 1999). The first module of IGENPRO is called PROTREN and it performs intelligent signal detection. Each individual signal trend is classified

as increasing, decreasing or constant. PROTREN is fuzzy-logic-based methodology to detect trends based on the information contained in the current and a few recent sample points such that timely and reliable trend information from incoming on-line signals is obtained. Instead of focusing on some specific feature as what is done in conventional methods, PROTREN's methodology extracts many statistical features from incoming signals, fuses them, and makes decisions through a fuzzy decision strategy

1.3 References:

1.1. Mormam J.A., Reifman J., Vitela J.E., Wei T.Y.C., Applequist C.A., Hippley P., Kuk W. and Tsoukalas L.H., "IGENPRO Knowledge-Based Digital System for Process Transient Diagnostics and Management," Proceedings of the IAEA Meeting on Advanced Technologies for Improving Availability and Reliability of Current and Future Water Cooled Nuclear Power Plants, Argonne, IL, September 8-11, 213-224, 1997.

1.2. Reifman J., "Survey of Artificial Intelligence Methods for Detection and Identification of Component Faults in Nuclear Power Plants," Nuclear Technology, 119, 76-97, 1997.

1.3. Reifman J., Wei T.Y.C., "PRODIAG: A Process-independent Transient Diagnostic System-I: Theoretical Concepts," Nuclear Science and Engineering, 131, 1-19, 1999.

2. OBJECTIVES AND TASKS

2.1 Objectives

The main objective of this research is to develop an improved fuzzy logic based detection method based on a comprehensive experimental testing program to detect reactor transients at the earliest possible time, practically at their birth moment.

The objectives of the research are:

- Substantially improve PROTREN to include more features such as higher order statistical moments, SPRT (sequential probability ratio testing), Bayesian inference.
- Develop separate effects experimental testing program and validate PROTREN using dynamic test data.
- Develop heat transfer experimental program and benchmark PROTREN transient detection method.
- Develop integral system testing of PROTREN using a scaled advanced boiling water reactor system and a small university nuclear reactor flux data.
- Develop prototype application of the PROTREN to detect incipient of transient.

2.2 Tasks

The following tasks are identified to meet the above said goals.

Task 1: Identification of Multiple Transients;

Task 2 More Efficient Detection Features;

Task 3 PROTREN with Non-Gaussian Noise;

Task 4 Trades off Between Conservative and Active Detection.

Task 5 Simulated Signal Testing;

Task 6 Experimental Data Testing;

Task 7 Systematic Comparisons and Validation;

Task 8 Benchmarking with Heat Transfer Data and

Task 9 Integral Facility Transient Testing.

3. PROTREN METHODOLOGY

2.1 PROTREN Description

Here the PROTREN's methodology is summarized.

The structure and general logic of the methodology is schematically illustrated in the flow chart of Figure 3.1, and the details can be found in a recent publication (Wang, 2001).

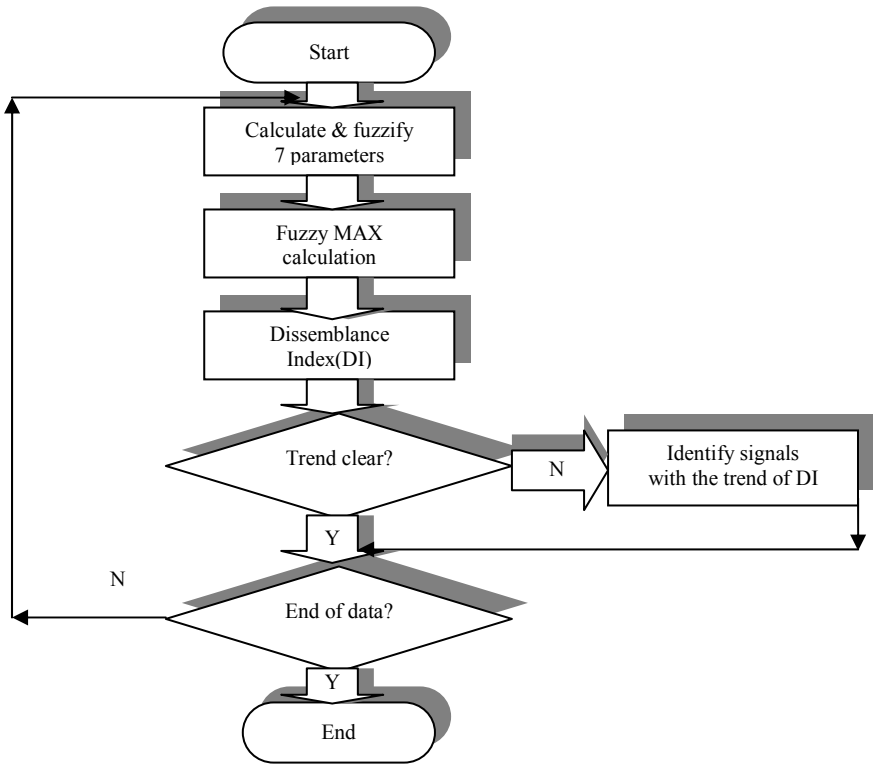

Figure 3.1. Flowchart of the fuzzy methodology

Seven statistical parameters extracted from the online signal are fuzzified, that is, their values are aggregated in fuzzy sets (Tsoukalas, 1997). These parameters, including pdf (probability density function), ex3 (the expected third moment), ravg (relative deviation), cum_pdf (cumulative probability density function), pdfofavg (probability density function of average value), avgd (average derivative), sd (sample derivative),

mom3 (the third moment) contain different signal characteristics respectively. The definitions of these parameters are described as follows:

(a) Probability density function (pdf)

$$pdf_{t_c} = \frac{1}{\sqrt{2\pi}\sigma} \exp^{-\frac{(s_{t_c}-\mu_s)^2}{2\sigma^2}} \tag{1}$$

where,

t_c =current time step

s_{t_c} =signal value at tc

μ_s =mean value of the steady-state signal

σ =standard deviation of the steady-state signal

(b) Cumulative probability density function (cum_pdf)

$$cum_pdf_{t_c} = \sum_{i=0}^{n} pdf_{t_{c-i}} \tag{2}$$

where,

n represents the length of the time window.

(c) Probability density function of average value($pdfofavg$)

$$pdfofavg = \frac{1}{\sqrt{2\pi}\sigma} \exp(-\frac{(avg-\mu)^2}{2\sigma^2}) \tag{3}$$

where,

$$avg = (\sum_{k=0}^{4} s_{t-k})/5 \tag{4}$$

μ_s =mean value of a steady-state signal

σ =standard deviation of a steady-state signal

s_{t-k} =the sample value k time steps before the current point

(d) Average derivative ($avgd$)

$$avgd_{t_c} = \left| \frac{wavg_{t_c} - wavg_{t_{c-1}}}{t_c - t_{c-1}} \right| \tag{5}$$

where,

$$wavg_{t_c} = \frac{\sum_{i=0}^{n}\left[e^{-k(t_c - t_{c-i})} s_{t_{c-i}}\right]}{\sum_{i=0}^{n} e^{-k(t_c - t_{c-i})}} \qquad (6)$$

s_{t-k} =the sample value k time steps before the current point

(e) Relative deviation ($ravg$)

$$ravg_{t_c} = \left|\frac{avg_{t_c} - \mu_s}{\mu_s}\right| \qquad (7)$$

where,

μ_s =mean value of a steady-state signal (assume mean value is not zero)

(f) Sample derivative (sd)

$$sd_{t_c} = \left|\frac{s_{t_c} - s_{t_{c-1}}}{t_c - t_{c-1}}\right| \qquad (8)$$

(h) The third moment (mom3)

$$mom\ 3 = \frac{\sum_{i=0}^{4} (s_{t_{c-i}} - \mu_s)^3}{5} \qquad (9)$$

t_c =current time step

s_{t_c} =signal value at tc

μ_s =mean value of the steady-state signal

In order to integrate all the information, the seven fuzzified parameters are synthesized into one final fuzzy number representing, in an approximate way, the degree to which the current constellation of features offers evidence for the onset of transient. At last, a fuzzy decision strategy is applied on the final fuzzy number and a trend identification decision is made. Preliminary test have been performed with simulated data and few actual plant data. Figures 3.2 and 3.3 show two flow signal data from the Chemical Volume Control System of a pressurized water reactor power plant sampled at 5 sec intervals. Figure 3.2 illustrates the changing pump discharge header flow and

Figure 3.3 illustrates the outlet flow of the letdown heat exchanger. The signals shown in Figure 3.2 and in Figure 3.3 are transient and constant respectively. For transient signal, PROTREN begins to provide the transient result in ten seconds after the transient onset, when the change is about 0.3%. For steady state signal, the response of PROTREN is correct and stable. It is apparent that the methodology does not deduce transients for steady state signals and can provide detection of transients for actual transient signals.

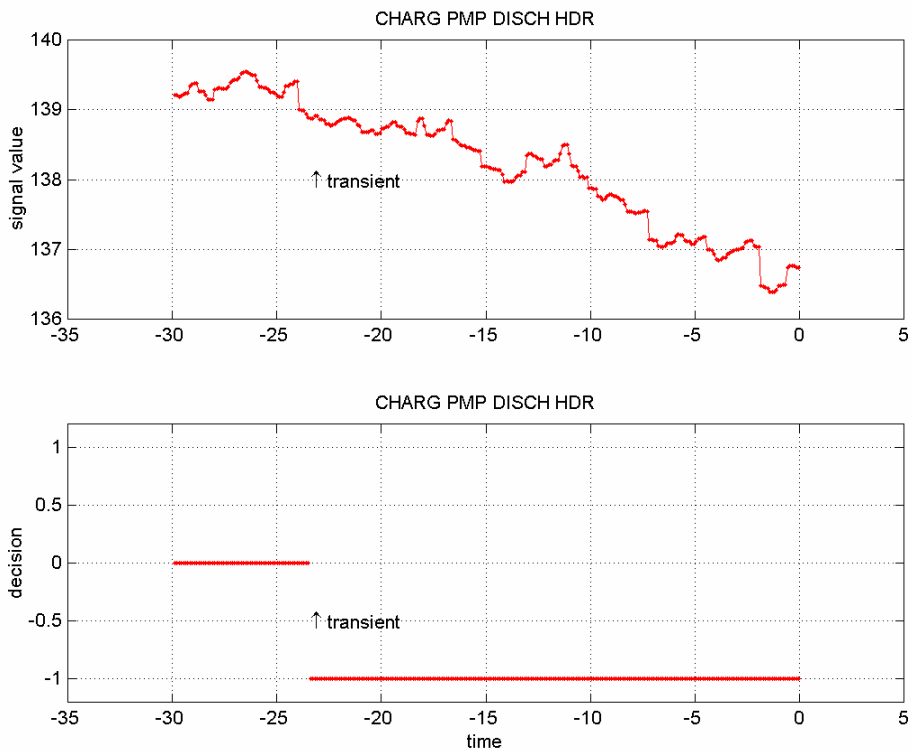

Figure 3.2 PROTREN results for a decreasing signal trend

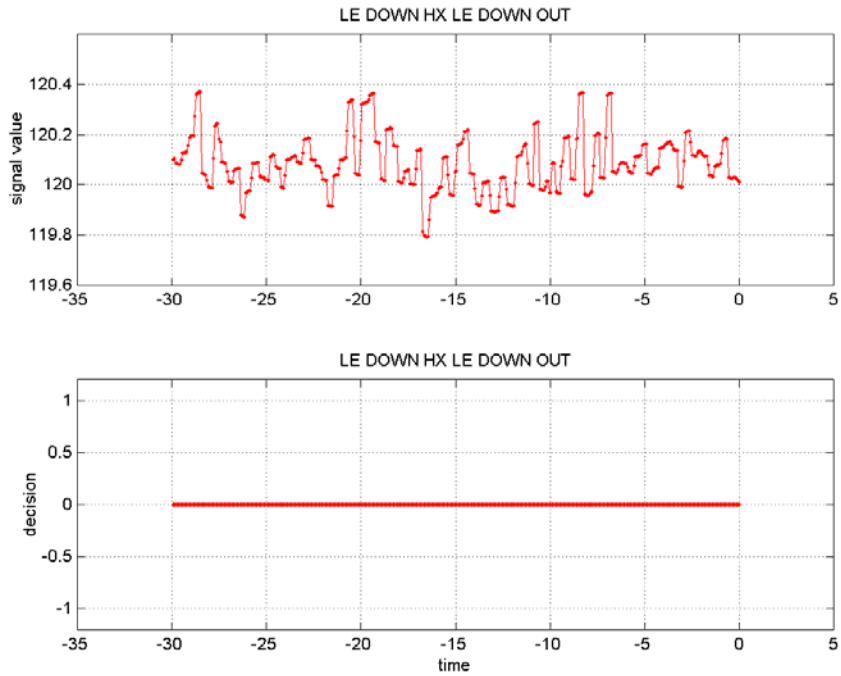

Figure 3.3 PROTREN results for an unchanging signal trend

However, several problems need to be solved before PROTREN can be applied to prototype applications. For example, PROTREN can only identify the first transient in the signal at this time, which is undesirable. In addition, conventional methods can be integrated into PROTREN as additional features. SPTR is one of such candidate. The classical binary SPRT is used to test a null hypothesis H0 and against the alternative hypothesis H1 about an unknown mean value of a Gaussian process. It is regarded as optimal from a statistical point of view. Given the limitation of false alarm and miss alarm, SPRT can detect the signal corrupted by Gaussian noise in the shortest time (Wald, 1947) (Racz, 1996). However, once the noise is not exactly Gaussian, which happens in most industrial processes, SPRT is far from optimal. For the signals corrupted by non-Gaussian noise, the performance of PROTREN may degrade significantly because of inappropriate choice of signal features. This research addresses these problems by proposing to improve, test, benchmark, and develop prototype application of PROTREN to reactor systems.

3.2 References

3.1. Kaufmann A., Madan M. Gupta, Introduction to Fuzzy Arithmetic: Theory and Application, New York, 1991.

3.2. Mormam J.A., Reifman J., Vitela J.E., Wei T.Y.C., Applequist C.A., Hippley P., Kuk W. and Tsoukalas L.H., "IGENPRO Knowledge-Based Digital System for Process Transient Diagnostics and Management," Proceedings of the IAEA Meeting on Advanced Technologies for Improving Availability and Reliability of Current and Future Water Cooled Nuclear Power Plants, Argonne, IL, September 8-11, 213-224, 1997.

3.3. Racz A., "Comments on the Sequential Probability Ratio Testing Methods," in Annals of Nuclear Energy, 23, No. 11, pp. 919-934, 1996.

3.4. Reifman J., "Survey of Artificial Intelligence Methods for Detection and Identification of Component Faults in Nuclear Power Plants," Nuclear Technology, 119, 76-97, 1997.

3.5. Reifman J., Wei T.Y.C., "PRODIAG: A Process-independent Transient Diagnostic System-I: Theoretical Concepts," Nuclear Science and Engineering, 131, 1-19, 1999.

4. THEORETICAL SIMULATION OF TWO PHASE FLOW

Monte-Carlo simulation has been developed to generate the various two phase flow regimes based on the liquid and gas flow rate and some assumptions. For this a single point conductivity probe was considered as an instrument in the diagnostic of two-phase flow in a vertical pipe. The conductivity probe, as a measuring tool inside a pipe line, has minimum flow intrusion and is simple to operate. As a first step in developing the diagnostic method, simulated signals of the probe were obtained at the pipe center line. A simple statistical technique, Sequential Probability Ratio Test (SPRT) was applied to the probe signal, and the on-line monitoring of two-phase flow transition was studied. In the present simulation we consider the cocurrent, vertical, upward two phase flow of air and water. For the vertical pipe, the upward two-phase flow is classified in flow patterns as bubbly flow, slug flow, churn flow and annular flow. These flow patterns are characterized by various void distributions. The bubbly flow pattern is distinguished by the presence of dispersed gas bubbles in a continuous liquid phase. The bubbles can be of variable size and shape. Slug flow is distinguished by the presence of gas plugs (or Taylor bubbles) separated by liquid slugs. The liquid film surrounding the Taylor bubble usually moves downward. Several small bubbles may also be dispersed within the liquid. The churn flow is more chaotic but of the similar characters as the slug flow. Annular flow is distinguished by the presence of a continuous core of gas surrounded by an annulus of the liquid phase. If the gas flow in the core is sufficiently high, it may carry liquid droplets. In this case the flow is referred as annular-dispersed (annular misty) flow. The liquid droplets are torn from the wavy liquid film, get entrained in the gas core, and can be de-entrained to join the film downstream of the point of their origin.

The simulation of the conductivity probe is carried out based on reliable theoretical two phase flow models such as the drift flux models and empirical correlations. The transitions between the two flow patterns were determined by the model proposed by Mishima and Ishii [6].

Based on the time traces obtained the signal processing was performed and the void fraction, transition time distribution and other further information can be obtained. This is the main approach for the simulation of conductivity probe signals.

4.1 Simulation of Bubbly Flow

Here for simplicity the bubbly flow is viewed as random distributions of small bubbles moving along the pipe. It is assumed that bubbles are spherical and their sizes vary within a small range. For the assumed average bubble size, a normal distribution was considered to account for bubble size variation. The bubbles are assumed to move with the constant speed, and the bubble breakup and coalescence are neglected. In figure 4.1, typical simulation geometry is shown.

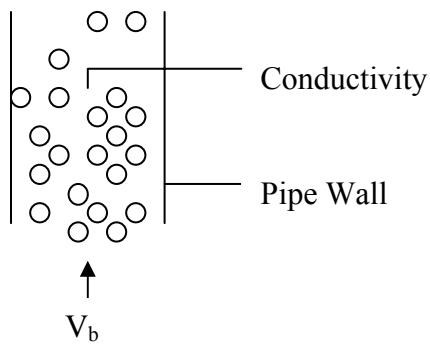

Figure 4.1.Bubbly Flow Simulation Geometry

For a given j_g and j_f, bubble rise velocity and void fraction can be determined using drift flux model [1],

$$V_b = 1.2\left(j_g + j_f\right) + 1.53\left(\frac{\sigma g \Delta\rho}{\rho_f}\right)^{0.25}(1-\alpha)^{1.75}$$
$$\alpha = \frac{j_g}{V_b} \qquad (4.1)$$

From void fraction and bubble rise velocity the time trace of conductivity probe is obtained by Monte-Carlo method, as explained below.

If T_g and T_f stand for the time that bubble and liquid pass through the conductivity probe as shown in Figure 4.2, then,

$$\sum_i T_{gi} = \alpha T \qquad (4.2)$$

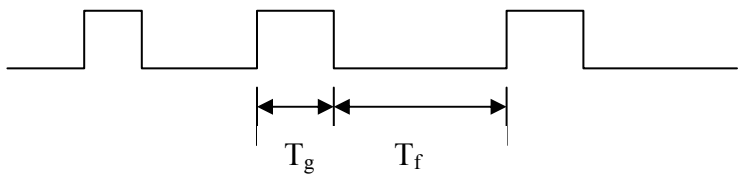

Figure 4.2. Idealized output voltage of conductivity probe

Where, T is total simulation time, and α is void fraction.

From Figure 4.3, the transition time (gas phase passing time) is calculated as,

$$T_{gi} = \frac{2\sqrt{r_b^{\,2} - r_i^{\,2}}}{V_b} = \frac{2r_b\sqrt{1-\xi^2}}{V_b} \qquad (4.3)$$

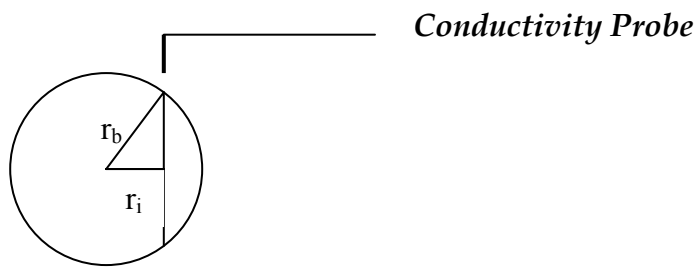

Figure 4.3 Schematic of spherical bubble and conductivity probe

where, r_i is the distance between conductivity probe and bubble center, and ξ is a random number in (0,1). Here bubble radius r_b is generated from a normal distribution around a mean bubble radius using Monte-Carlo method. The liquid passing time T_{fi} is assumed to have a Poisson distribution [2], and is also generated by Monte Carlo method. Thus the following relationship can be written for liquid phase passing time,

$$\sum_i T_{fi} = (1-\alpha)T \qquad (4.4)$$

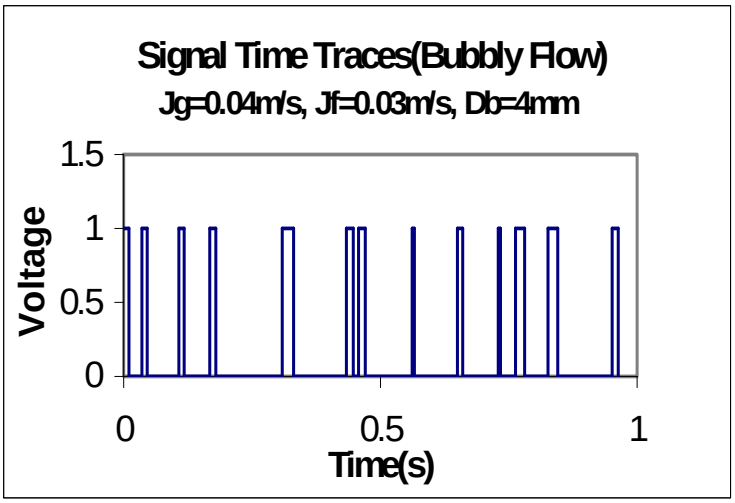

Figure 4.4 Signal time traces for Bubbly Flow

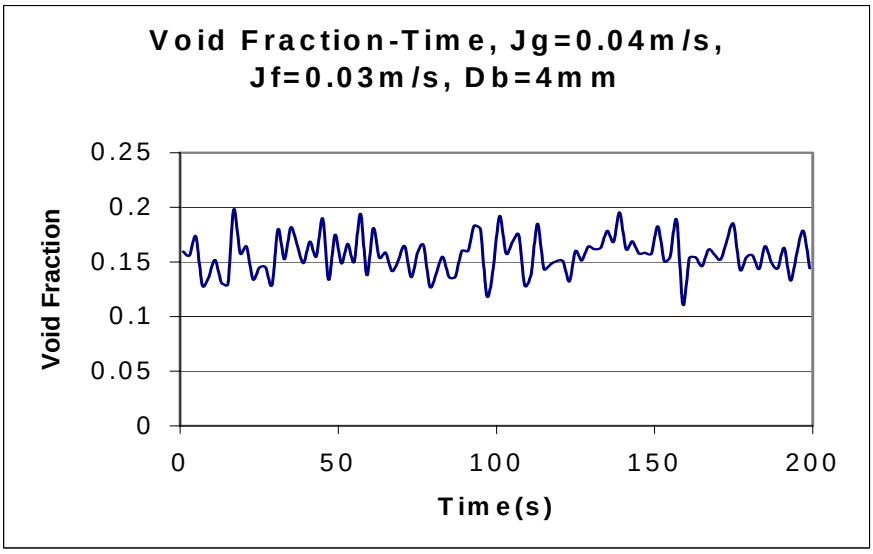

Figure 4.5. Void fraction time traces for Bubbly Flow
(Ts is average time for void fraction calculation)

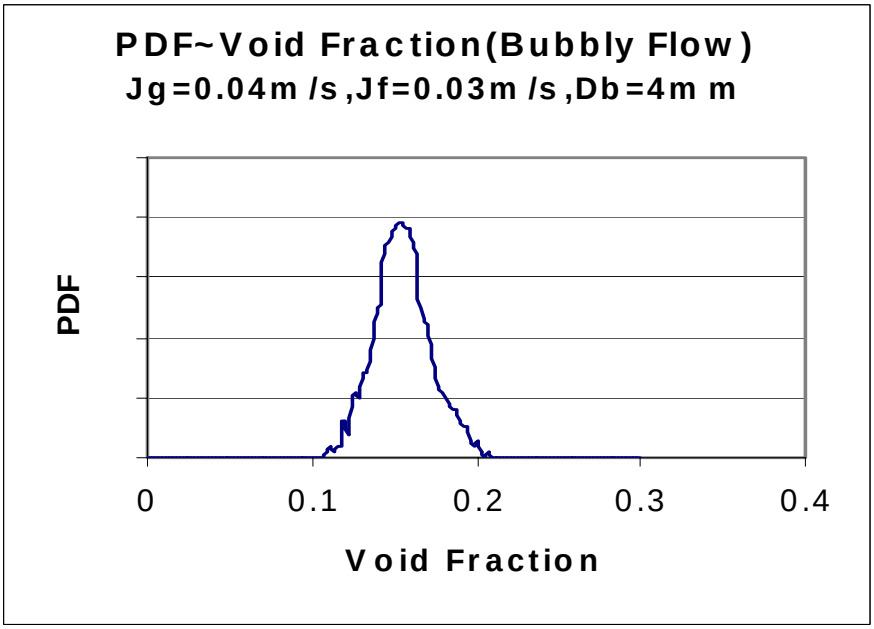

Figure.4.6. PDF of void fraction for Bubbly Flow

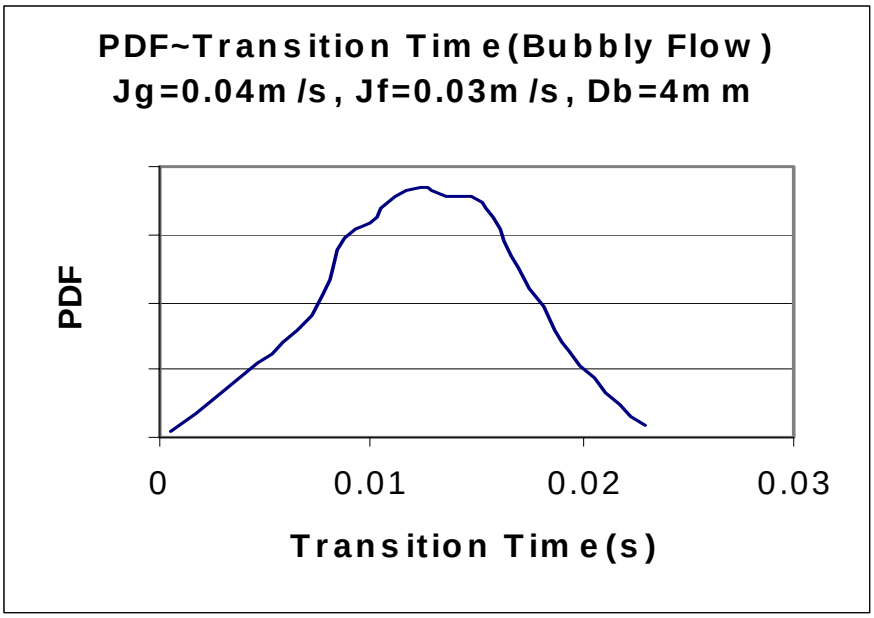

Figure.4.7. PDF of transition time for Bubbly Flow

From T_{gi} and T_{fi}, the time trace of conductivity probe signal is obtained. The typical time trace of probe signal is shown in Fig 4.4. From the probe signal, the void fraction is obtained by Eqn. (4.2). In Fig.4.5, the local void fraction time trace is shown. In the case T=1second was used as the sampling time. The flow pattern characteristics can be easily seen through the probability density function (PDF) of void fraction and transition time. In Fig.4.6, the PDF of void fraction is shown. The PDF shows a peak at the mean void fraction around 0.15. In Fig.4.7, the PDF of the bubble passing time is shown. The maximum bubble passing time corresponds to the maximum bubble radius. The PDF of the transition time is an important parameter which helps in detecting different sizes of bubbles in the flow, (and hence maybe in the transition of flow from one phase to another), even when the flow is of a constant void fraction.

4.2. Simulation of Slug Flow

The slug flow is characterized by consecutive slug units which consist of a large Taylor bubble and a liquid slug. The liquid slug region is geometrically similar to bubbly flow. In the simulation, the average size of spherical bubbles in the liquid slug is assumed to be 4mm in diameter. The simulation for the liquid slug is the same as for bubbly flow pattern. The liquid slug length for fully developed slug flow is relatively insensitive to the values of j_g and j_f. Griffith et al[3] and Akagawa et al[4] have given that the average length of liquid slug is 8D(D is the pipe diameter), while Barnea et al[5] have shown that

$$L_b = \frac{nD\ V_{TB} + j_g L_s}{mV_{TB} - j_g}$$

the mean slug length varied between 10D to 15D. Here it is assumed that the liquid slug length has a Gaussian distribution with mean value of 12D and a range between 8D-16D

The mean Taylor bubble length is calculated as [3],

where, D is the pipe diameter, L_s is the liquid slug length and V_{TB} is the Taylor bubble rise velocity given by:

$$V_{TB} = 1.2\,j + 0.35\sqrt{gD}$$

The values of constant m and n used are recommended by[3]:

$$m=0.913, \quad n=0.526, \quad \text{for } L/D<20.$$

The minimum length of Taylor bubble in slug flow is taken as 2D [5]. The maximum Taylor bubble length was determined by the transition slug bubble length L_b

$$\sqrt{\frac{2\Delta\rho g L_b}{\rho_f}} = j + 0.75\sqrt{\frac{\Delta\rho g D}{\rho_f}}\left(\frac{\Delta\rho g D^3}{\rho_f \gamma_f^2}\right)^{1/18}$$

by Mishima and Ishii[6], and is given in the following expression:

Here for the lengths of liquid slug and Taylor bubble, mainly experimental results are employed. There were also some theoretical models such as Fernandes et al[7], Orell et al[8] and Ishii et al[9] for slug flow pattern. However, there are some discrepancies between these models and between models with experimental results. Thus, here the geometric consideration for slug flow unit is mainly based on the experimental results.

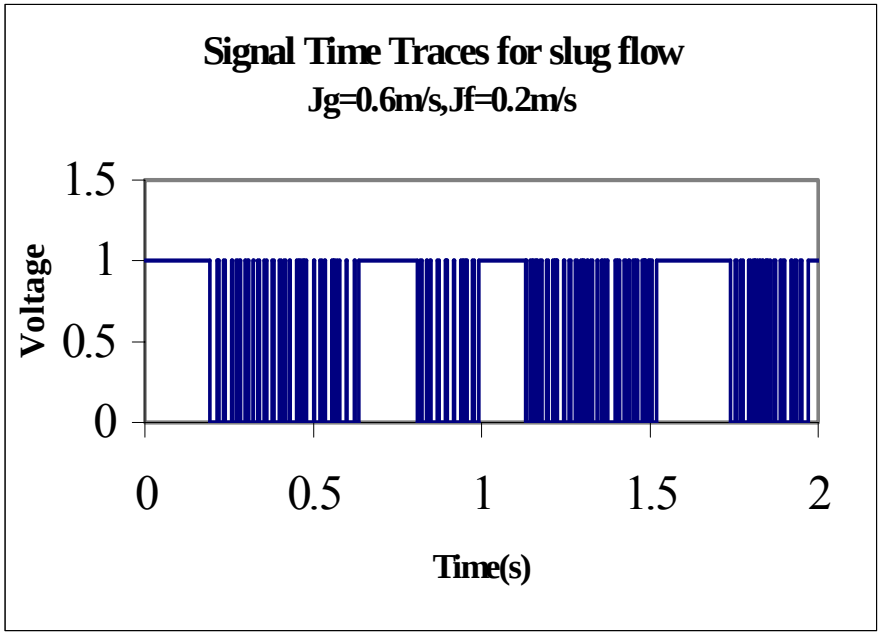

Figure.4.8. Signal time traces for Slug Flow

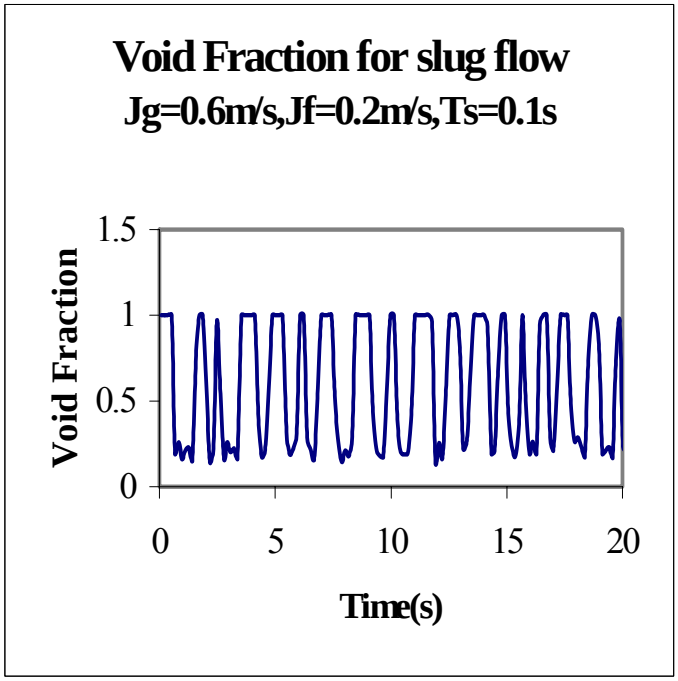

Figure.4.9. Void fraction time traces for Slug Flow
(Ts is average time for void fraction calculation)

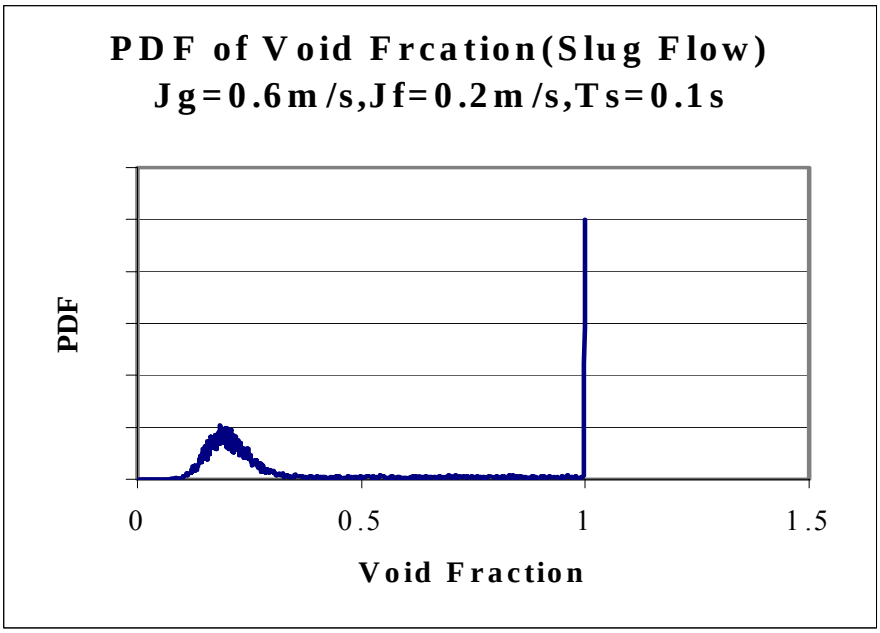

Figure.4.10. PDF of Void fraction for Slug Flow
(Ts is average time for void fraction calculation)

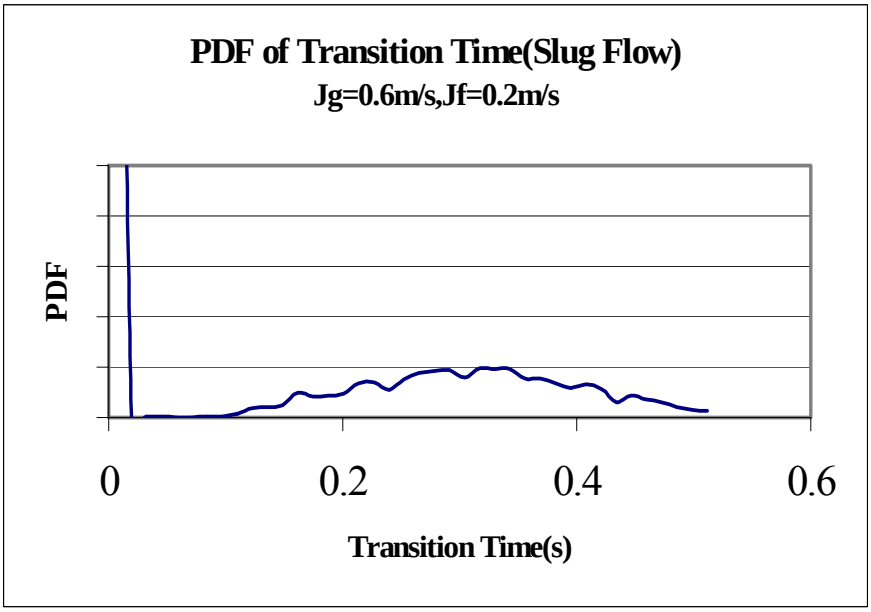

Figure.4.11. PDF of transition time for Slug Flow

In addition, the simulation is constrained by the void fraction consideration [6] shown below:

$$\alpha = j_g / V_{TB}$$
$$\alpha_B = 1 - 0.813\ X^{0.75},\ X \equiv f(L_B)$$
$$\alpha L = \sum_i (\alpha_{Bi} L_{Bi} + \alpha_{Si} L_{Si})$$

where, L is the total length of the slug flow and α is the overall void fraction in L; L_B and L_S are lengths of Taylor bubble and liquid slug, respectively; α_B and α_S are void fraction of the Taylor bubble unit and liquid slug unit, respectively.

Based on the geometric distribution and void fraction consideration, the time traces of the probe signal for slug flow is obtained and shown in Fig.4.8. Note, the large intervals correspond to the Taylor bubble passing times. In Fig.4.9, the void fraction time trace is shown. The void fraction can reach 1.0 since the sampling time is 0.1 second. Furthermore, the distributions for void fraction and transition time are also obtained. In Fig.4.10, the PDF of void fraction is shown. The two peaks correspond to the Taylor bubbles and small spherical bubbles respectively. The PDF of transition time is shown in Fig.4.11. The small bubbles have a high and sharp distribution while the Taylor bubbles possess a low and flat PDF.

4.3. Simulation of Churn Flow

Churn flow is somewhat similar to slug flow. However, it's much more chaotic, frothy and disordered. The bullet-shaped Taylor bubble becomes narrow, and its shape is distorted. The continuity of the liquid in the slug between successive Taylor bubbles is repeatedly destroyed by a high local gas concentration in the slug. Typical of churn flow is the oscillatory or alternating direction of motion of the liquid. The highly agitated liquid flow makes churn flow look like the most complex flow in vertical test section. Here the churn flow is treated as an extension of slug flow for the simulation,. Based on the geometrical characteristics of the churn flow, it is assumed that there is also a typical

unit that consists of a liquid slug and a Taylor bubble. The liquid slug is similar to bubble flow where the void fraction is about 0.25. The consecutive connections between two units are so random that the liquid slug may not exist. The Taylor bubble length is assumed less than that in slug flow pattern. The geometric distribution of the gas and liquid phase is given below.

For the maximum length of the Taylor bubble, Mishima & Ishii's correlation [6] for the

Taylor bubble length in transition region was employed. The expression is,

$$\sqrt{\frac{2\Delta\rho g L_b}{\rho_f}} = j + 2.25\sqrt{\frac{\Delta\rho g D}{\rho_f}}$$

where L_b is the maximum length of the Taylor bubble and the Taylor bubble length is assumed uniformly distributed from 0 to the maximum value.

$$L_b\alpha_b + L_s\alpha_s = L\alpha$$

For the liquid slug, the mean length satisfied the expression below:

The average void fraction in liquid slug is assumed to be 0.25. The void fraction in Taylor bubble region is given by the same equation as that for the slug flow Taylor

$$V_{TB} = \frac{j_g}{\alpha} = 1.2(j_g + j_f) + \sqrt{2}\left(\frac{\Delta\rho g\sigma}{\rho_f^2}\right)^{0.25}$$

bubble. The bubble rise velocity in churn flow pattern is specified by Mishima & Ishii's correlation [6] and expressed below:

Based on the geometrical distribution of the two phase flow, the time traces of probe signal for churn flow is obtained and shown in Fig.4.12. In Fig.4.13, the void fraction fluctuation is shown. The void fraction and transition time distribution (PDF) are shown in Fig.4.14 and Fig.4.15. In Fig.4.14, there is only one peak near the void fraction 1.0 since the sampling time 0.2 seconds is bigger than liquid slug passing time.

4.4. Simulation of Annular-misty Flow

It is not necessary to simulate for annular flow if the conductivity probe is located in the centerline of the pipe, since only gas phase passes through. For the annular misty flow, the simulation can be conducted similar to bubbly flow pattern. The continuous phase is gas and the dispersed phase is liquid for Annular misty flow while for bubbly flow vice verse. Similar to the simulation for bubbly flow, the droplet size, droplet velocity and void fraction are determined at first.

For the liquid droplet size, Hinze [10] gave a Weber number criteria for critical droplet

$$D_{vm} = 0.028 \frac{\sigma}{\rho_g j_g^2} Re_f^{-1/6} Re_g^{2/3} \left(\frac{\rho_g}{\rho_f}\right)^{-1/3} \left(\frac{\mu_g}{\mu_f}\right)^{2/3}$$

diameter. Here in the simulation, the liquid droplet size is given by Kataoka-Ishii [11] droplet size model which is a mechanistic correlation based entrainment mechanism of the shearing off of the wave crest and the wave undercut. The volume median diameter is:

By the carefully experimental study, Ishii and Zhang et al [12] gave a modified upper-limit log-normal distribution for droplet size D_p:

$$f = \frac{dV}{Vdy} = \frac{\xi}{\sqrt{\pi}} e^{-\xi^2 y^2},$$

$$y = ln\left[\frac{\left(D_{max}^p - D_{vm}^p\right)}{D_{vm}^p} \frac{D_p}{(D_{max}^p - D_p)}\right]$$

where, D_{max} is the maximum stable droplet diameter and D_{vm} is the volume median droplet diameter. From the experiment study, $D_{max}=4.0D_{vm}$, p = 3, and ξ =0.25.

The droplet velocity is given by the drift flux model [1] and expressed as:

$$V_{dj} = \frac{(1-\alpha)(1-E_d)}{\alpha + 4\sqrt{\rho_g / \rho_f}}\left[j + \sqrt{\frac{\Delta\rho g D(1-\alpha)(1-E_d)}{0.015\rho_f}} \right]$$

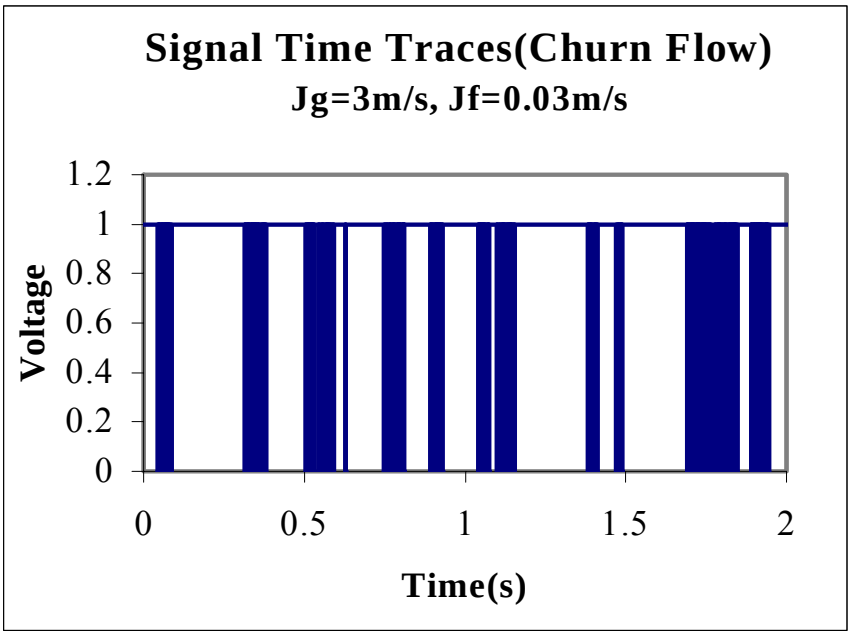

Figure.4.12. Signal time traces for Churn Flow

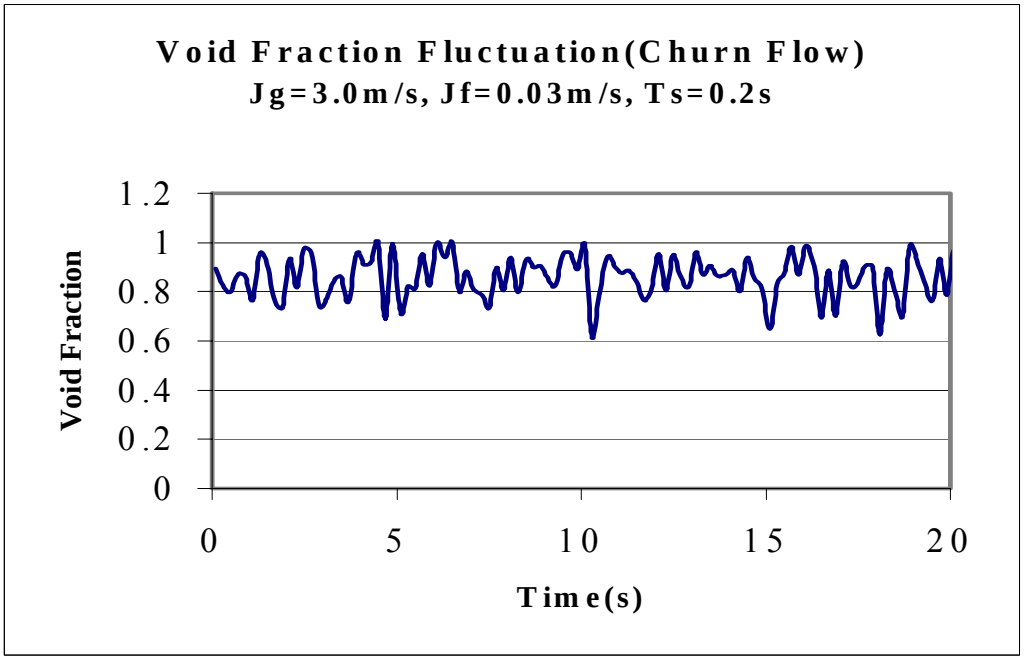

Figure.4.13. Void fraction time traces for Churn Flow
(Ts is average time for void fraction calculation)

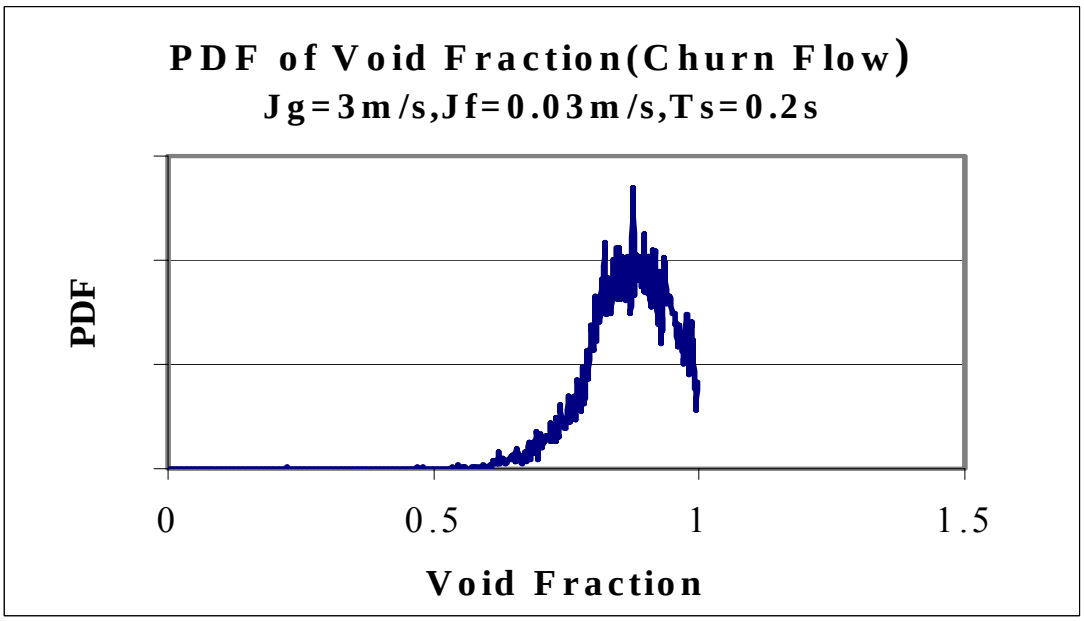

Figure.4.14. PDF of Void fraction for Churn Flow
(Ts is average time for void fraction calculation)

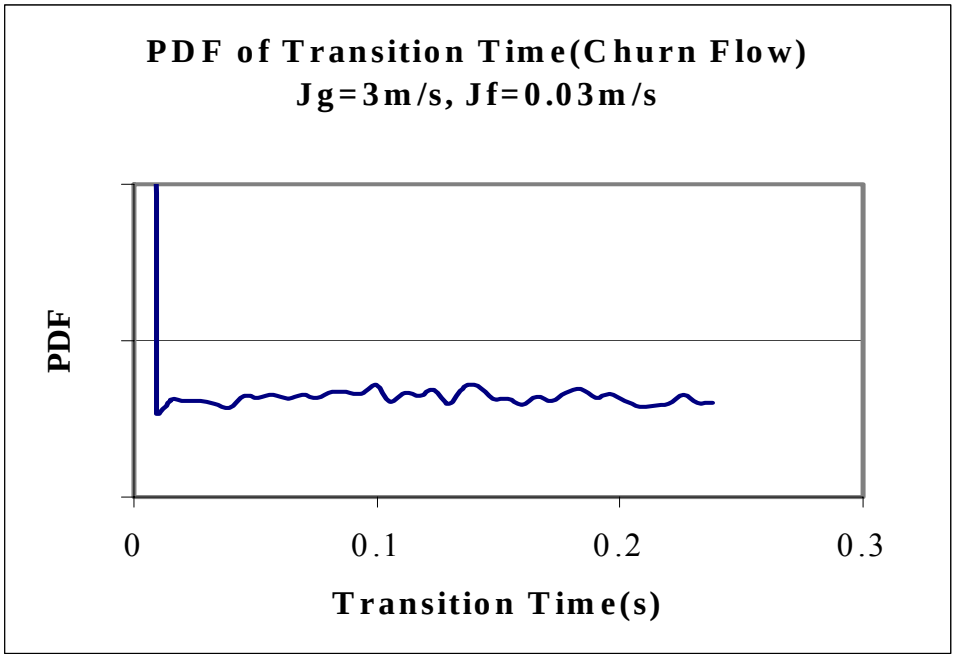

Figure.4.15. PDF of transition time for Churn Flow

The void fraction is given by Mishima&Ishii [6] model,

$$V_{gj} = \frac{(1-\alpha)(1-E_d)}{\alpha + 4\sqrt{\rho_g / \rho_f}}\left[j + \sqrt{\frac{\Delta\rho g D (1-\alpha)(1-E_d)}{0.015\ \rho_f}} \right]$$

$$+ \frac{E_d(1-\alpha)}{\alpha + E_d(1-\alpha)} \times \frac{3\sigma}{\rho g}\left[\frac{(g\Delta\rho)^2}{\mu_g \rho_g} \right]^{\frac{1}{3}} \frac{1}{j^2}$$

After the droplet size, droplet velocity and void fraction are specified, the simulation is performed similar to bubbly flow. The simulation results are shown in Fig.4.16 to Fig.4.19.

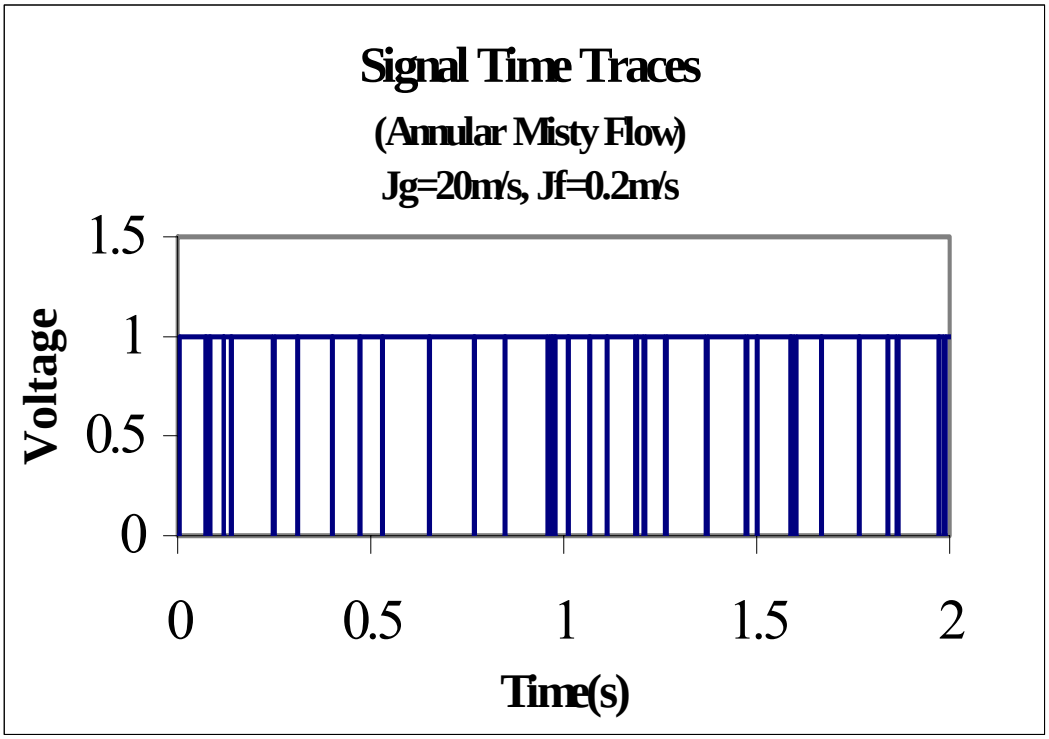

Figure.4.16. Signal time traces for Annular-Misty Flow

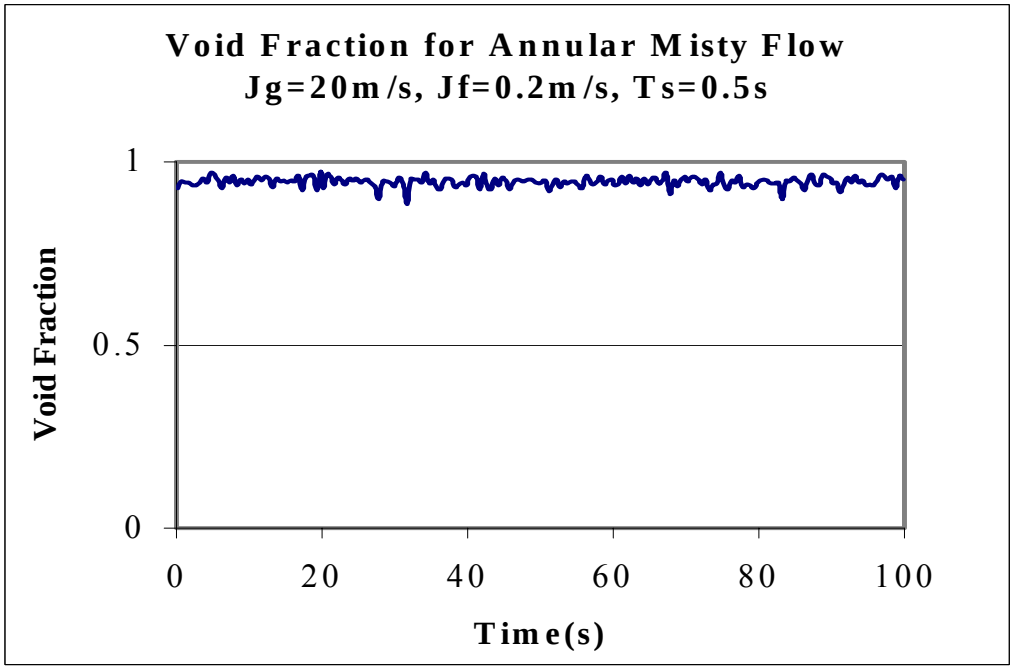

Figure.4.17. Void fraction time traces for Annular-Misty Flow

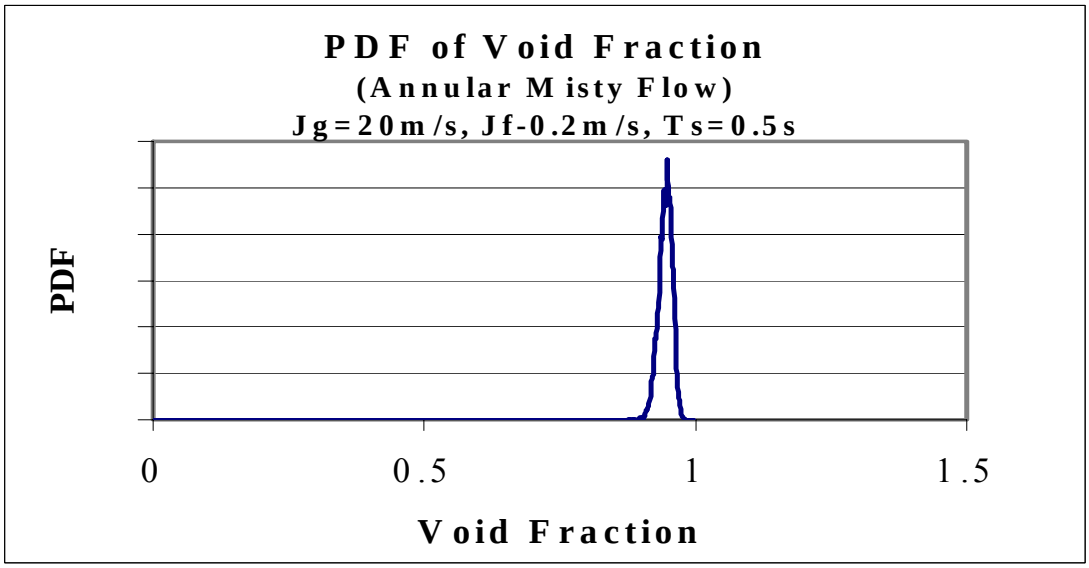

Figure.4.18. PDF of Void fraction for Annular-Misty Flow

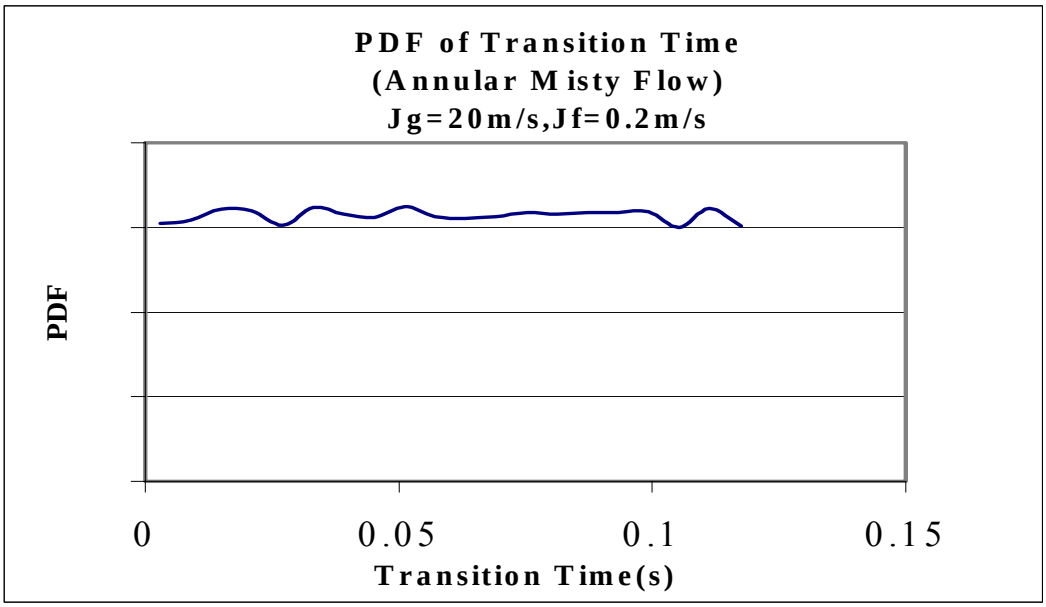

Figure.4.19. PDF of transition time for Annular-Misty Flow

4.5 SPRT for On-Line Diagnosis of Flow Pattern Recognition.

In the previous sections, the flow pattern characteristics were identified by the probe signal. For dynamic detection of the flow pattern, the SPRT method is used. The probe signal is first processed for void transit time. The signal is then subjected to the SPRT. The SPRT testing is carried out dynamically so that the flow detection is almost instantaneous. The principle of SPRT is described followed by the SPRT approach.

4.5.1. SPRT Method.

Here the SPRT method is briefly described. Details can be found in references [13-15]. Consider the problem of discriminating between two simple hypotheses:

$$H_0: \theta = \theta_0,\ H_1: \theta = \theta_1,\ \theta_0 \neq \theta 1; \qquad (4.5.1)$$

In this case, it is considered for the family $F_n(X_n;\ \theta)$, $\theta = \theta_0,\ \theta_1$ (i.e. the cumulative distribution function of the observations $x_1, x_2, \ldots x_n$ given the parameter θ) containing only two distinct distributions. Define,

α = probability that H_1 is chosen when H_0 is true;

$1 - \alpha$ = probability that H_0 is chosen when H_0 is true;

β = probability that H_0 is chosen when H_1 is true;

$1 - \beta$ = probability that H_1 is chosen when H_1 is true;

n = number of observations required to accept either H_0 or H_1

The terms α and β are called "error probabilities" and are usually determined by the nature of the problem and n is the "sample number".

The SPRT S (b,a) for the equation (4.5.1) is defined by the following: Observe the sequence of observations $\{xi\}$(i = 1,2,…) successively, and at stage $n \geq 1$,

1. Accept H_0 if $Z_n \leq b$;
2. reject H_0 if $Z_n \geq b$;
3. continue by observing X_{n+1} if $b < Z_n < a$

where stopping bounds (b,a) ($-\infty < b < a < \infty$) are two real numbers and Z_n is the natural logarithm of the probability ratio at stage n.

$$a = \ln(\frac{1-\alpha}{\beta}), b = \ln(\frac{\alpha}{1-\beta}) \tag{4.5.2}$$

$$Z_n = \ln \frac{f_n(X_n;\theta_1)}{f_n(X_n;\theta_0)} \tag{4.5.3}$$

The inequality $b < Z_n < a$ is called the "critical inequality" of S(b,a) at stage n. The sample number n at which a decision is made is called the "average sample number" (ASN) and depends upon the observations themselves and the value of θ. In many cases, the ASN can be computed as a function of θ and is denoted by E(n;θ).

There are a number of statistical tests to approach this problem. A "good" test should accept H_0 when θ is close to θ_0 and reject H_0 (accept H_1) when θ is close to θ_1 with high probability. Following Wald's sequential analysis [13] a decision test based on the SPRT has an optimal property; i.e. for given error probabilities, there is no other procedure with at least as low error probabilities or expected risk with shorter average sampling time than the SPRT. Because of this property and its inherent simplicity, the SPRT was chosen as the flow pattern annunciation tool.

4.5.2. Test Approach

First the simulation for all flow patterns was performed and the conductivity probe signals were obtained for the two – phase vertical flow. From the conductivity probe signals, transition time and the void fraction distribution were obtained. Since the transition time corresponds to the das phase geometry and carries instantaneous phase information, the SPRT was based on transition time distribution. As a first approximation, the transition time is assumed to have a normal distribution. If the transition time is non-Gaussian, the performance of SPRT using Gaussian Distribution is significantly affected.

The natural logarithm of probability likelihood ration SPRT(n) was calculated as

$$
\begin{aligned}
&SPRT(n) = Z_n = \ln(U_n) \\
&U_n = \frac{f_n(X_i/\theta_1)}{f_n(X_i/\theta_2)} = \prod_{i=1}^{n} \frac{f\,(X_i/\theta_1)}{f\,(X_i/\theta_2)} \\
&f_n(X_i/\theta_j) = (\sigma_j\sqrt{2\pi})^{-1}\exp[-(2\sigma_j{}^2)^{-1}(X_i - m_j)^2 \\
&\Rightarrow SPRT(n) = \sum_{i=1}^{n}[\frac{(t_i - m_2)^2}{2\sigma_2{}^2} - \frac{(t_i - m_1)^2}{2\sigma_1{}^2}] + n\ln(\frac{\sigma_2}{\sigma_1})
\end{aligned}
\tag{4.5.4}
$$

Where m_j and σ_j are mean and standard deviation for the transition time of the flow pattern j. m_1 and σ_1 are obtained on a long time run for steady state flow pattern 1. m_2 and σ_2 are renewable valus from the start of the test. t_i is the transition time sequence of the flow pattern.

Here in order to reduce the effect of sudden change in individual SPRT due to transition time fluctuations, the sampling interval, which is the number of the gas phase in this interval, was introduced. The sampling time interval corresponds to the actual sampling time given for given flow conditions through jg and jf. In this simulation, by counting the total gas phase number in a given time, the sampling intervals can be converted to sampling time.

Two average methods were used for obtaining SPRT. One is average SPRT which takes the average value of SPRT based on the individual transition time in sampling interval. The other method is SPRT based on average transition time. Comparisons of these two SPRT methods and the flow parametric study for flow pattern transition are presented in the following sections.

4.5.3. Test Results

4.5.3.1 Comparison between two SPRT methods

A comparison between two SPRT mehods is performed with the same flow conditions. In Fig. 4.20, the comparison for the transition between bubbly and slug flow is shown. The sampling interval is 25. The corresponding sampling times are shown in the figure. Before bubble sequence 40, the flow pattern is bubbly flow and the flow rates are jg = .03 m/s and jf = 0.03 m/s. The average bubble size is 4mm. The corresponding sampling time is 2.62s. From bubble sequence 40 – 120 a change in flow rate(jg = .06m/s and jf = .03m/s is introduced in the same size bubbles. Here, at bubble sequence

80, the mean and standard deviation values for the flow pattern 1 are updated by using the corresponding values of flow pattern 2. After bubble sequence 120, the flow pattern is slug flow (jg = .12m/s and jf = .03m/s). The threshold is -2.9 which corresponds to α and β = .05 (this is a 95% confidence level).From fig. 4.20, it is clear that there is almost no difference between the two SPRT methods. The SPRT value is not sensitive to the flow rate change within the bubbly flow, but is sensitive to the flow pattern transition to slug flow. This is due to the longer transition times for the slugs as compared to the bubbles.

Figs. 4.21 and 4.22 show the comparison of the two SPRT methods for the transition between bubbly, cap and slug for different sampling interval.

The average SPRT and the SPRT based on the transition time have similar performance; however the average SPRT shows more sensitivity to flow condition change than the latter. Furthermore, the sensitivity of SPRT increases when the sampling interval decreases.

4.5.3.2. Parametric study of SPRT for flow pattern transition

The test using two SPRT methods for different parameters such as the flow rate, sampling interval, cap bubble size and frequency, threshold was performed and the results shown in Figs 4.23 to 4.40The parametric study for the different sampling interval and flow rate (jg and jf) were performed for two flow classes; (1) bubbly flow with different flow rates and (2) slug to churn transition.

The test results in detection of different flow rates in bubbly flow are shown in fig 4.23 to 4.28. Figure 4.23 shows the results for a short sampling interval 10 by using average transition time SPRT. Here, it is noticed that when jf is increased to .06m/s with jg still .03m/s, the SPRT threshold is reached after a long time. On the other hand, when jg is changed keeping jf same, there is almost no change in SPRT. The SPRT values are more sensitive to the liquid flow rate than the gas flow rate for bubbly flow. The reason is that the gas flow rate strongly affects void fraction while the liquid flow rate affects the bubble rise velocity. The gas phase transition time is directly related to the bubble rise velocity while it is not so sensitive to the void fraction change. As the sampling interval increases the sensitivity of SPRT decreases.

The SPRT results for the slug to churn flow transition are shown in Fig 4.29 to 4.34. Fig. 4.29 shows the test results for slug and churn flow transition using SPRT based on average transition time. Here, the sampling interval is 10 and the threshold is -2.9. Four different groups of slug and churn flow were tested. In this case, the SPRT is more sensitive to the gas flow rate than the liquid flow rate. The reason is that due to the high void fraction, the gas flow rate strongly affects the bubble sizes and thus transition times. Fig. 4.30 shows the average SPRT result for the same test conditions as Fig. 4.29. The average SPRT is more sensitive is more sensitive than the SPRT based on transition time. The sensitivity of SPRT decreases as the size of the sampling interval increases. Thus a small sampling interval should be used for the slug to churn flow transition. Moreover, a large update period should be used due to the large fluctuation of transition time for slug to churn flows.

The two SPRT methods were studied with different cap sizes, cap frequencies and different thresholds for three flows – bubbly, cap and slug. Fig 4.35 and 4.36 show the test results for the different cap sizes using SPRT based on average transition time and average SPRT method respectively. As expected, the SPRT shows a change when the cap bubble size increases. Fig. 4.37 and 4.38 show the test results for the different cap bubble frequencies. Here, three groups of cap bubble flow with cap frequency ranging from 1/5 to 1/20 were introduced. It is clear from these figures that the SPRT is more sensitive when the cap bubble frequency increases. Figs. 4.39 and 4.40 show the SPRT test with different thresholds (-2.2, -2.9, -3.6). Here, the threshold of -3.6 corresponds to a 97.5% confidence level and -2.2 correspond to a 90% confidence level. The SPRT is more sensitive with a small confidence level.

Thus it is seen that SPRT responds very rapidly to sudden changes in signal level, or it will automatically extend its sequence length to detect very subtle changes in signal quality. To reduce the over sensitivity of SPRT, an average process in a sampling interval can be introduced. The parameters, including sampling interval, update period and the SPRT threshold should be properly selected depending on the flow pattern.

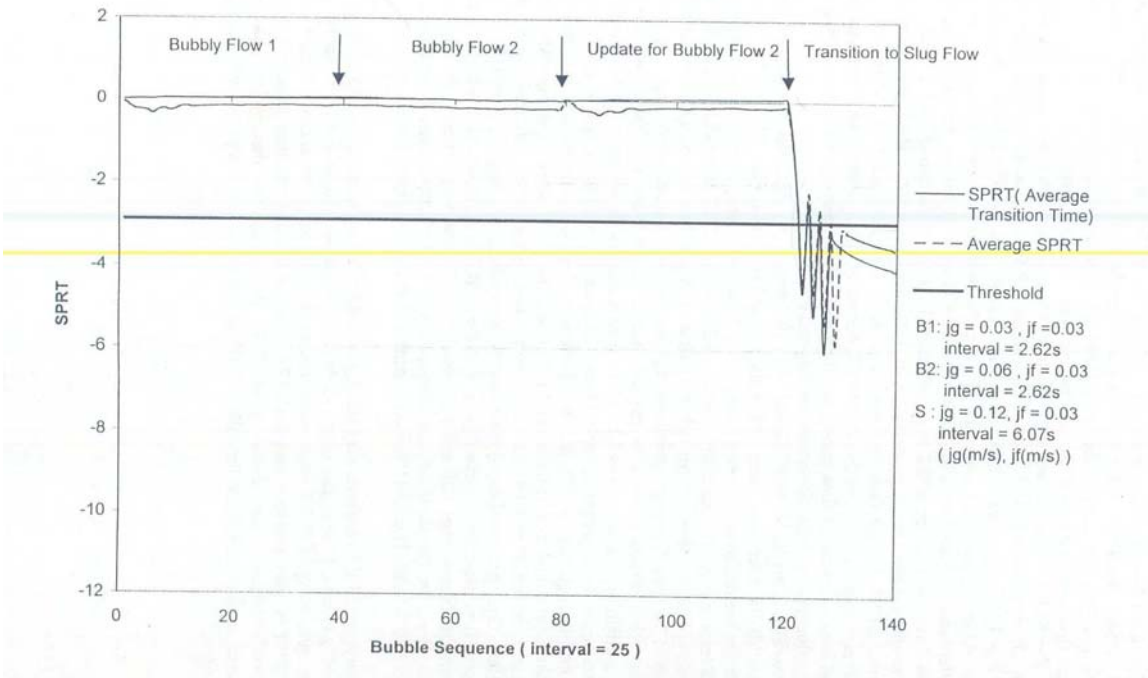

Figure. 4.20. Comparison of two SPRT methods for the transition between bubbly and slug flow.

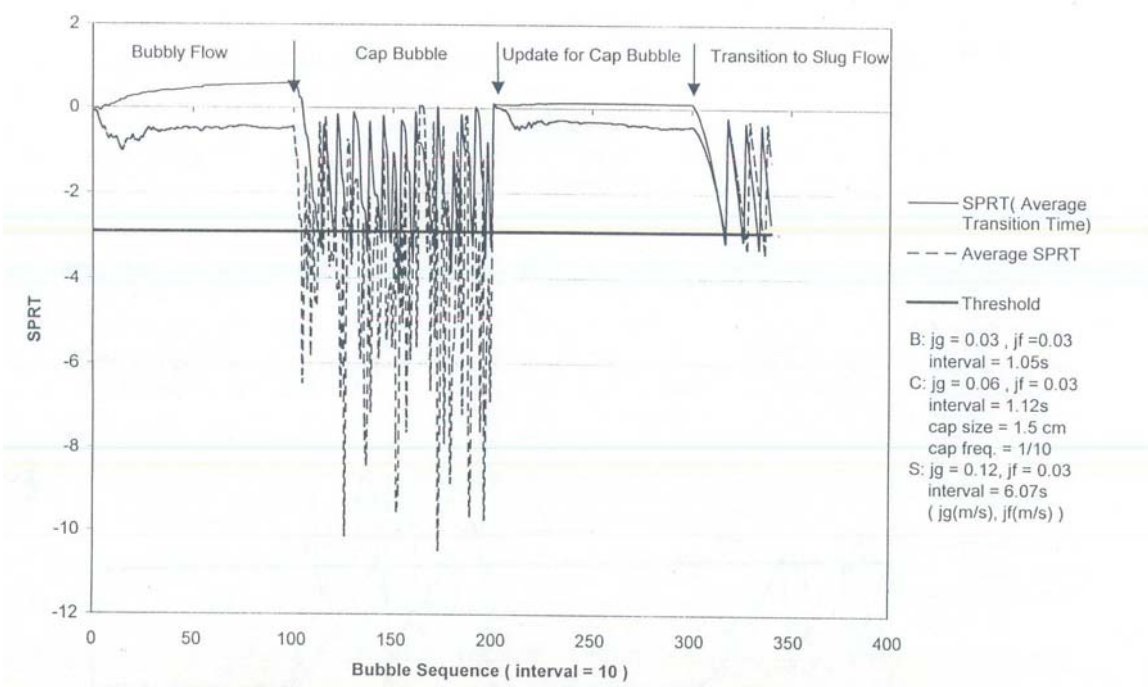

Figure. 4.21 Comparison of two SPRT methods for the transition between bubbly, cap and slug flow.

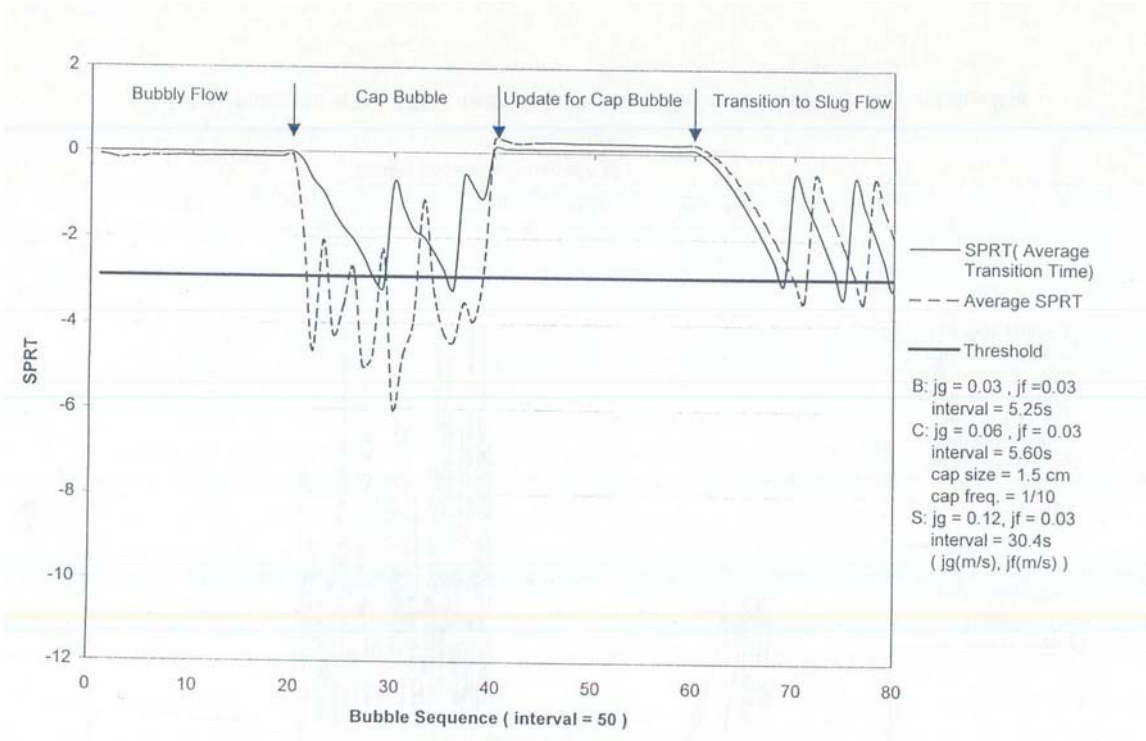

Figure. 4.22. Comparison of two SPRT methods for the transition between bubbly and slug flow.

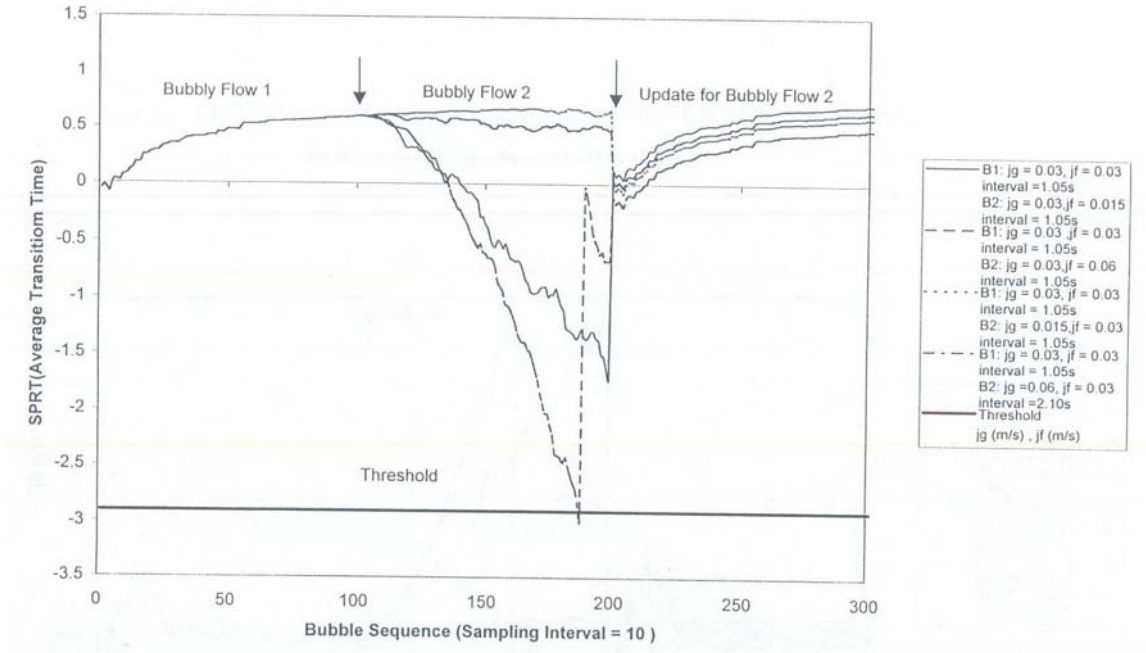

Figure. 4.23 Detection of change of gas/liquid flow rate in bubbly flow using SPRT based on average transition time.

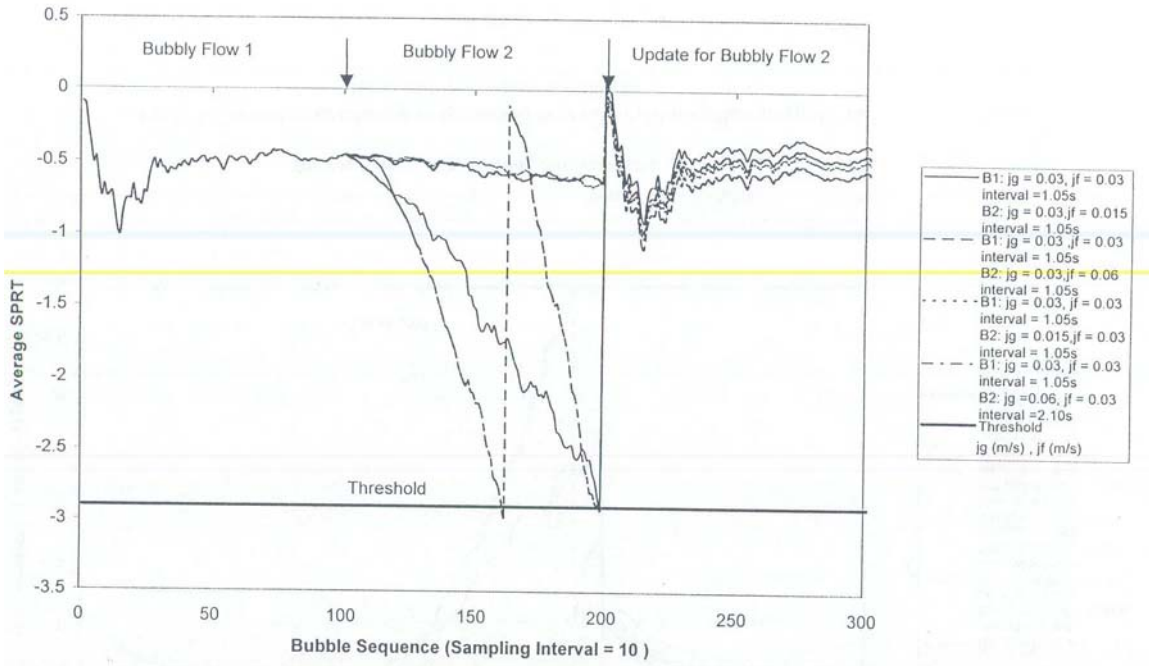

Figure. 4.23 Detection of change of gas/liquid flow rate in bubbly flow using average SPRT.

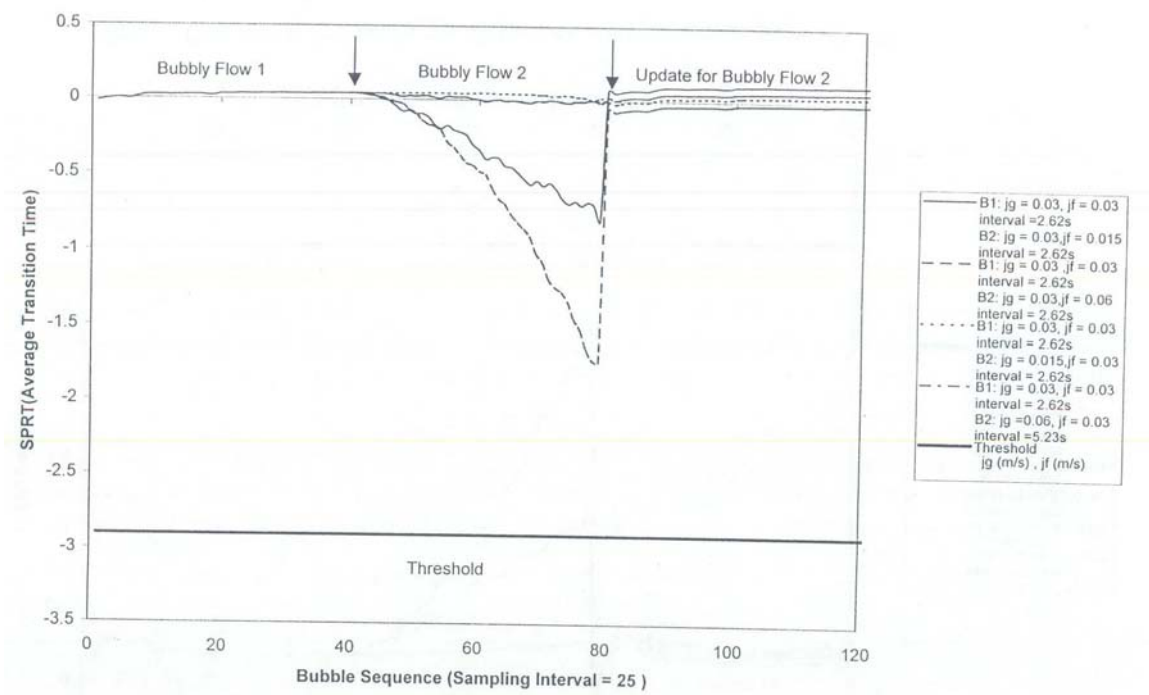

Figure. 4.24 Detection of change of gas/liquid flow rate in bubbly flow using SPRT based on average transition time.

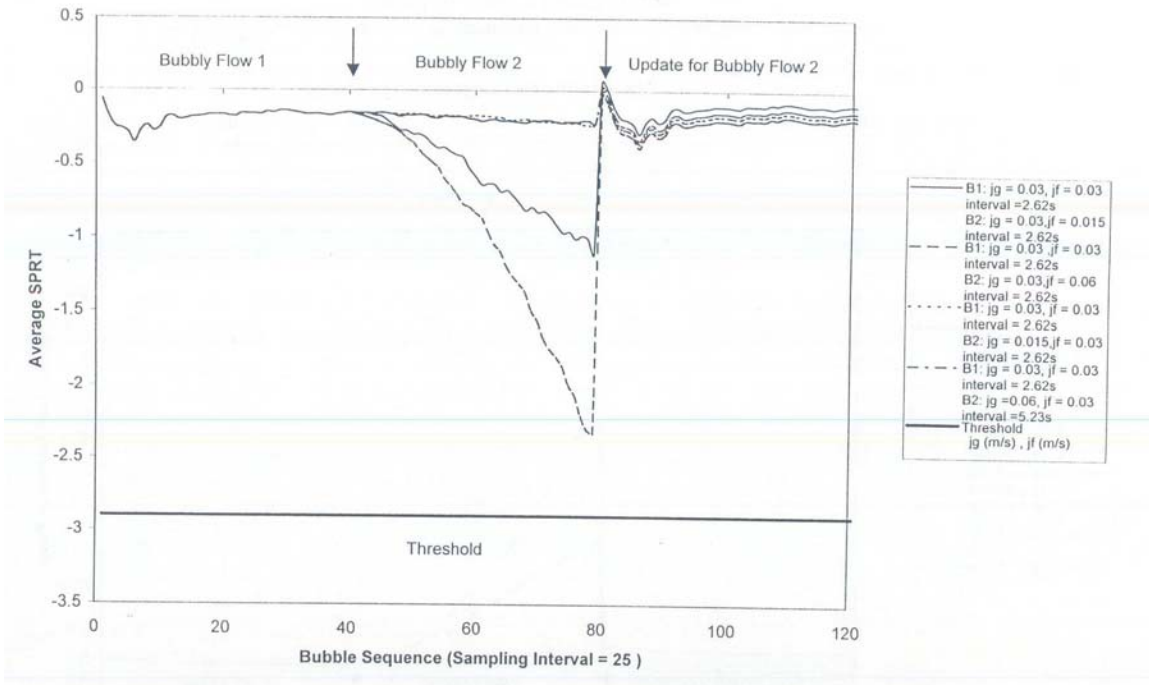

Figure. 4.25 Detection of change of gas/liquid flow rate in bubbly flow using average SPRT.

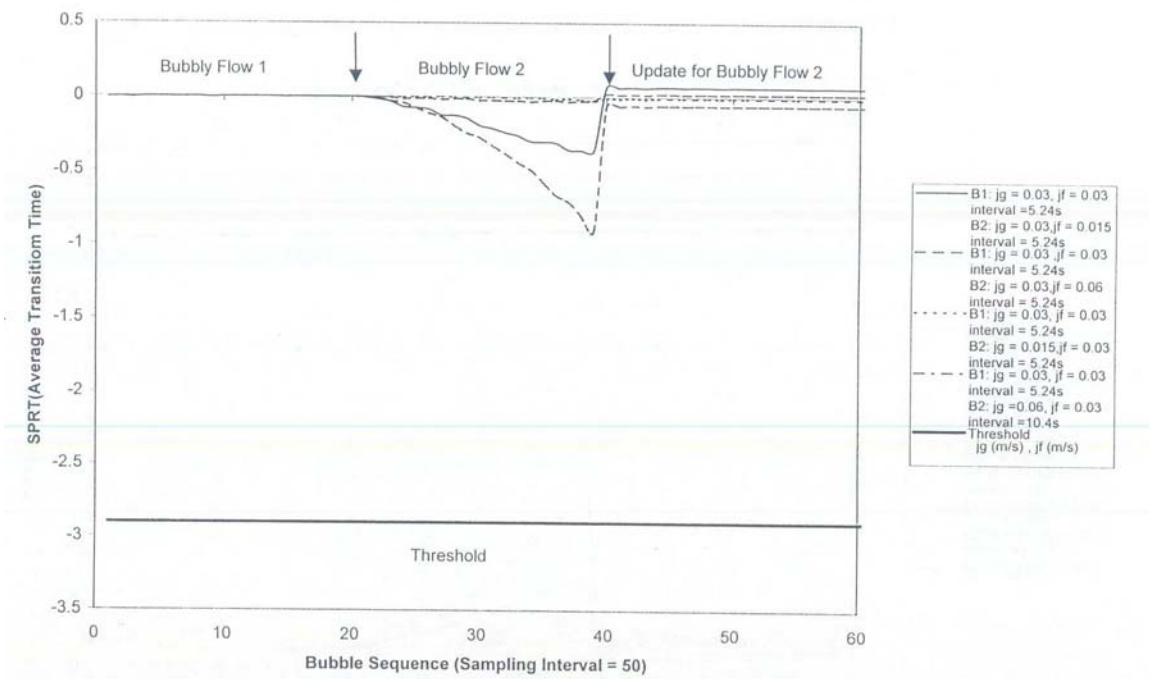

Figure. 4.26 Detection of change of gas/liquid flow rate in bubbly flow using average SPRT.

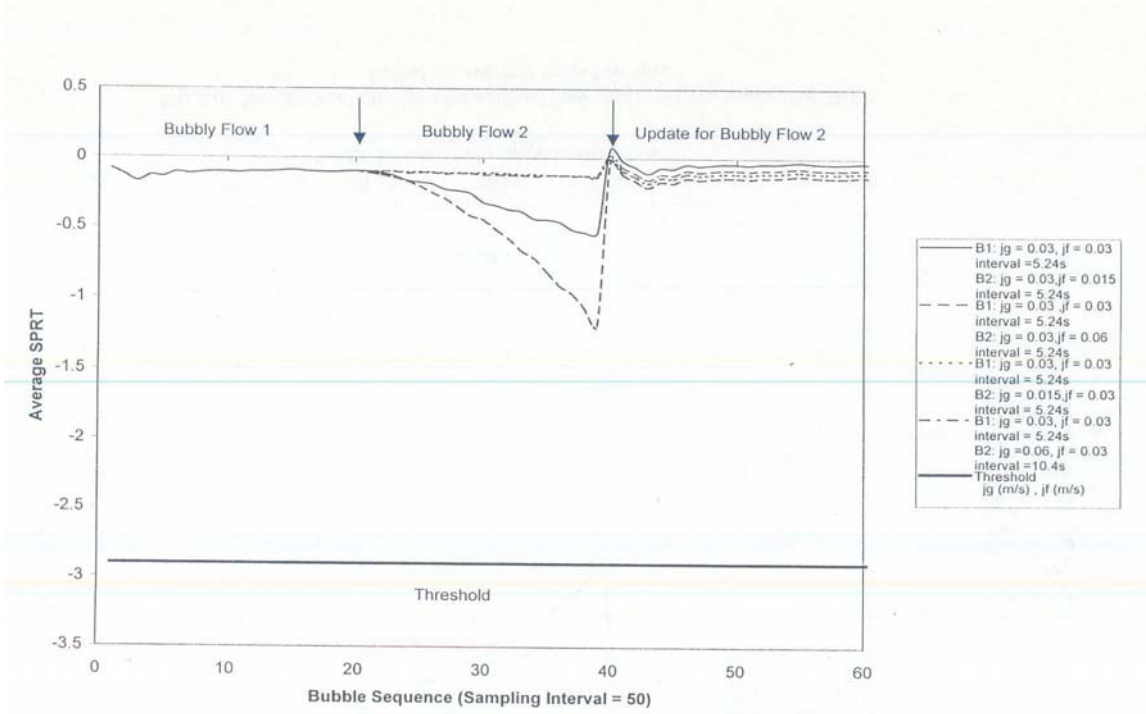

Figure. 4.27 Detection of change of gas/liquid flow rate in bubbly flow using SPRT based on average transition time.

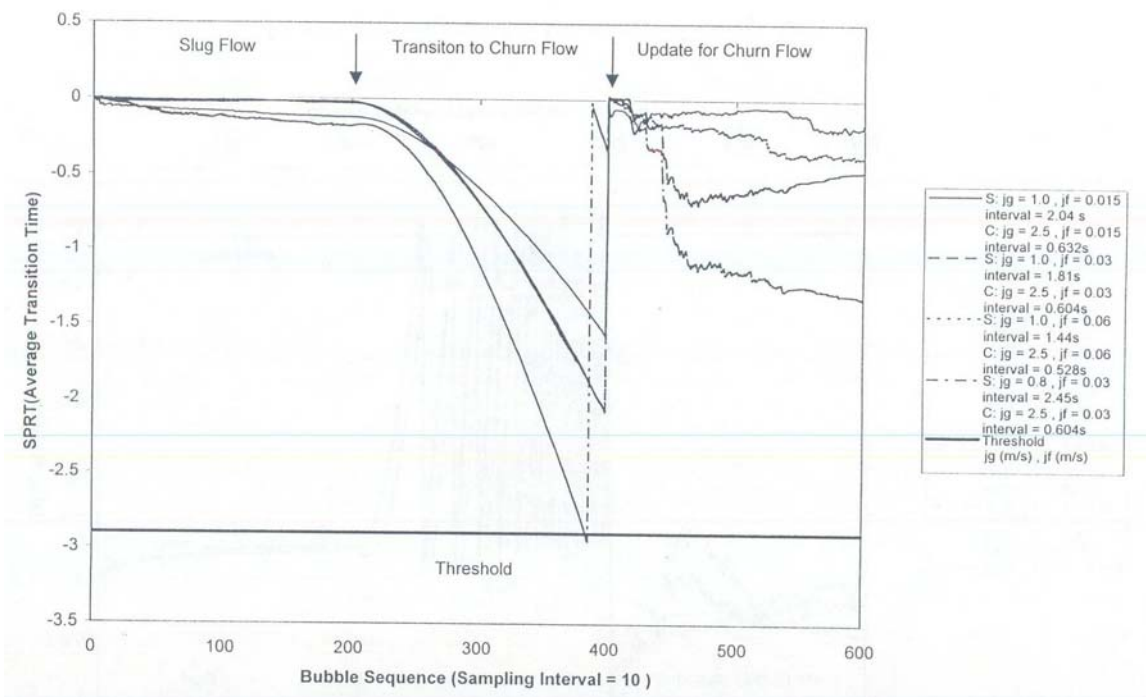

Figure 4.29 Slug and churn flow transition using SPRT based on average transition time.

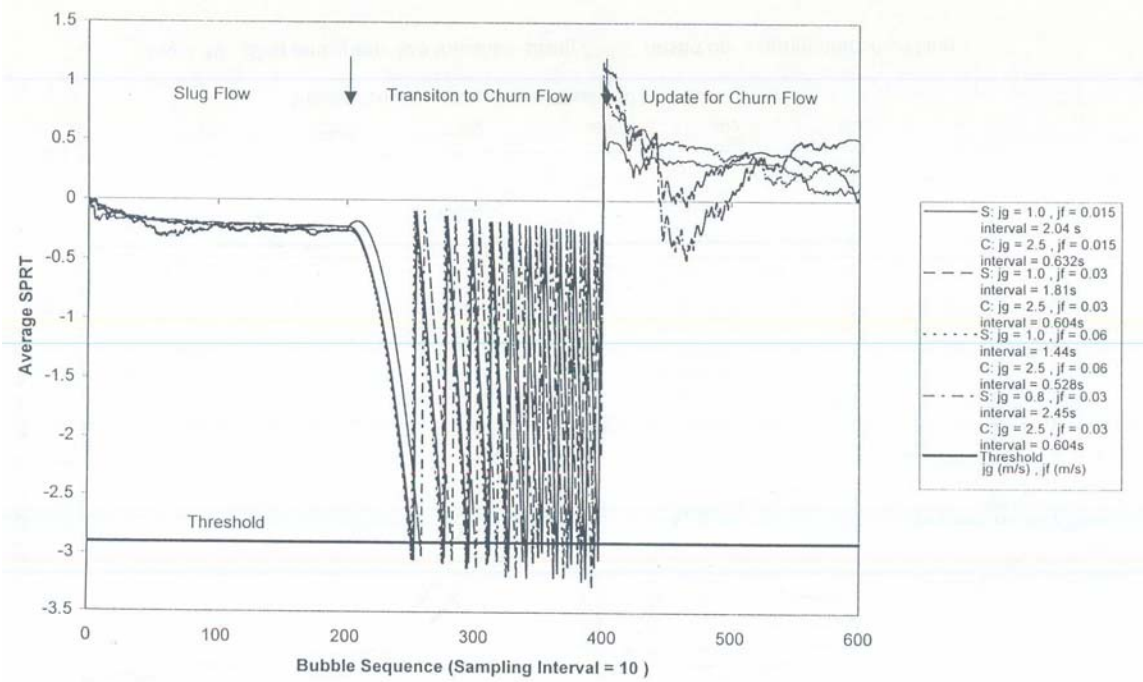

Figure 4.30 Slug and churn flow transition using average SPRT.

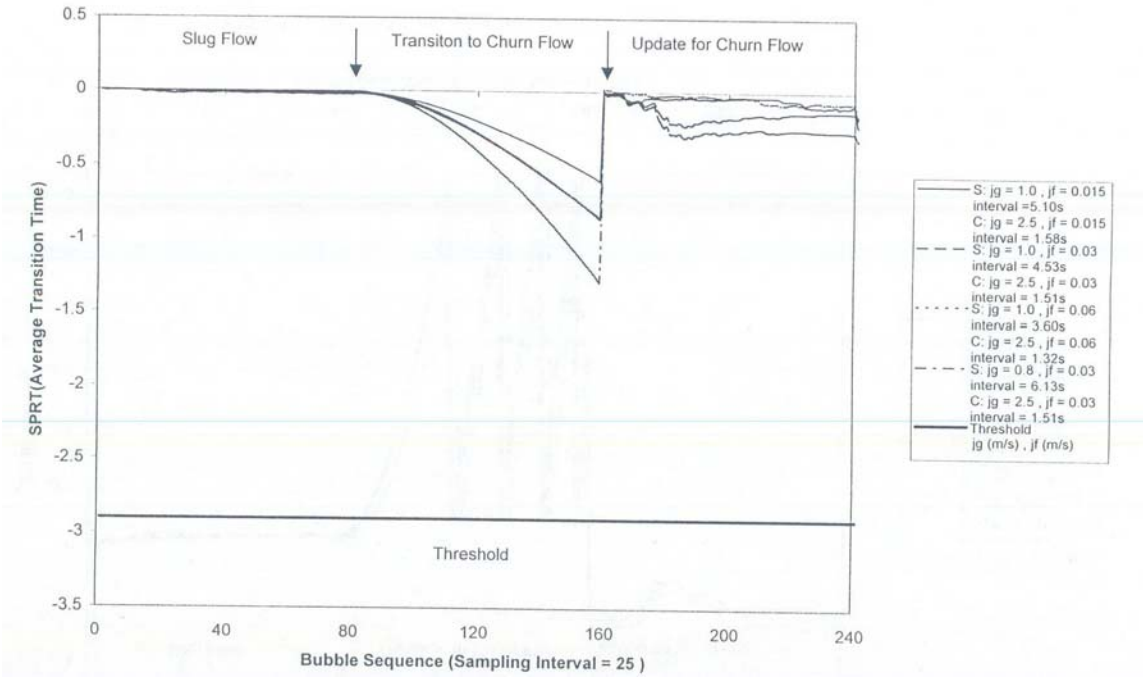

Figure 4.31 Slug and churn flow transition using SPRT based on average transition time.

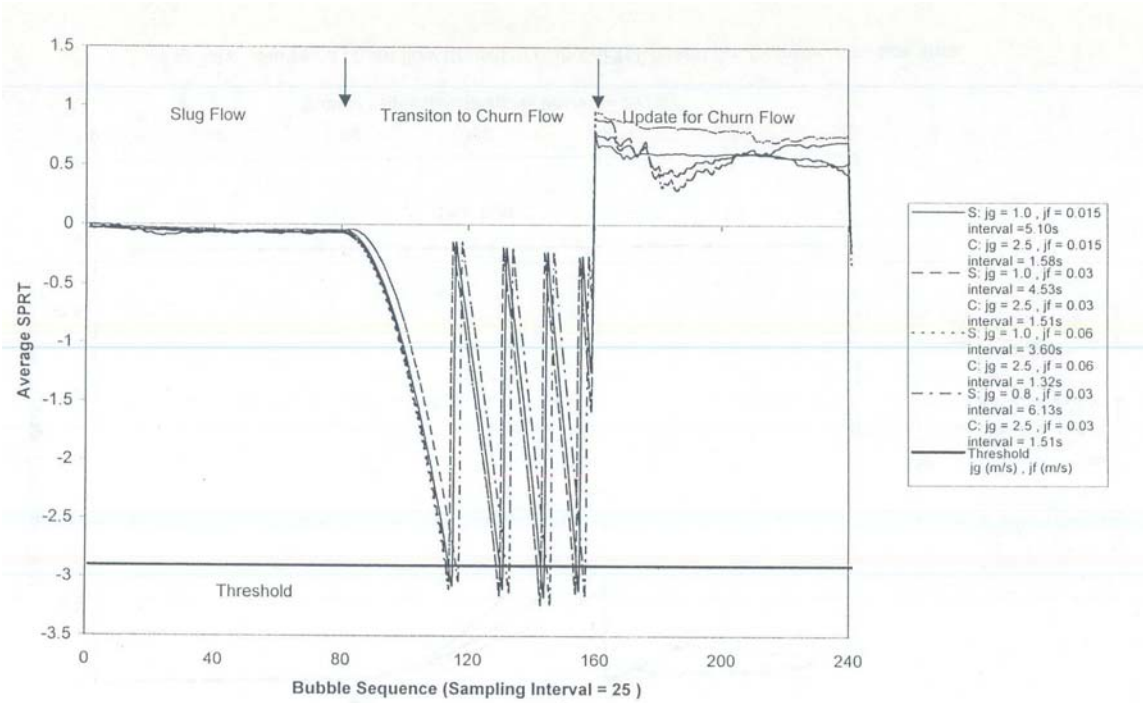

Figure 4.32 Slug and churn flow transition using average SPRT.

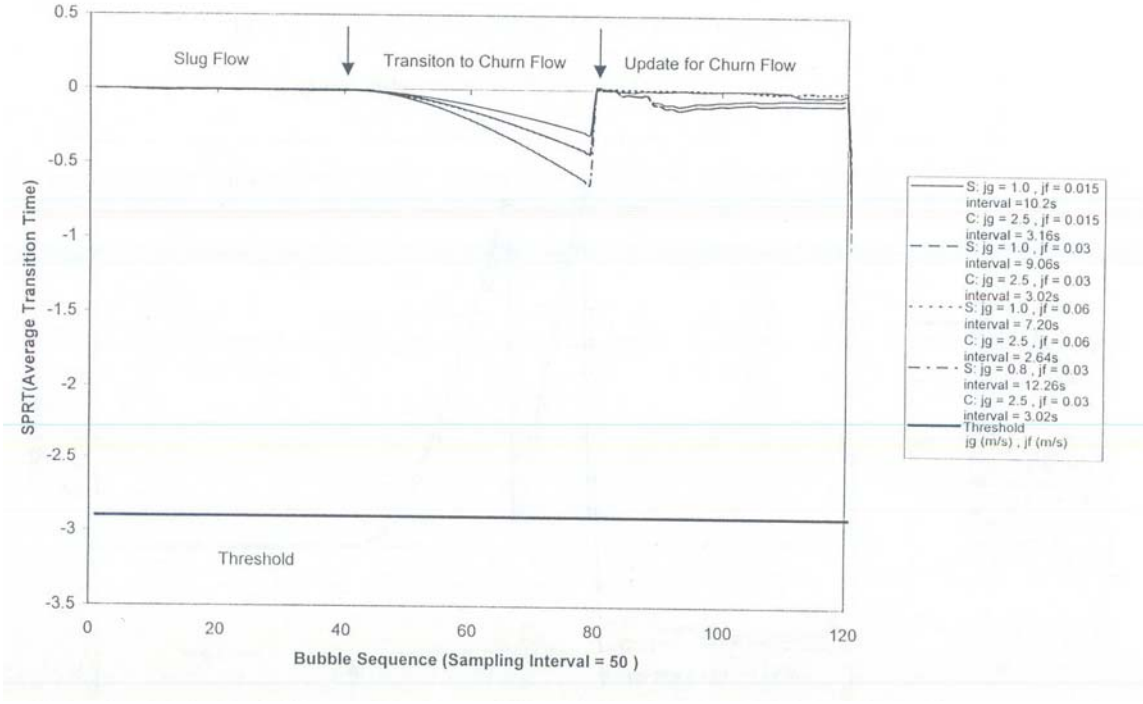

Figure 4.33 Slug and churn flow transition using SPRT based on average transition time.

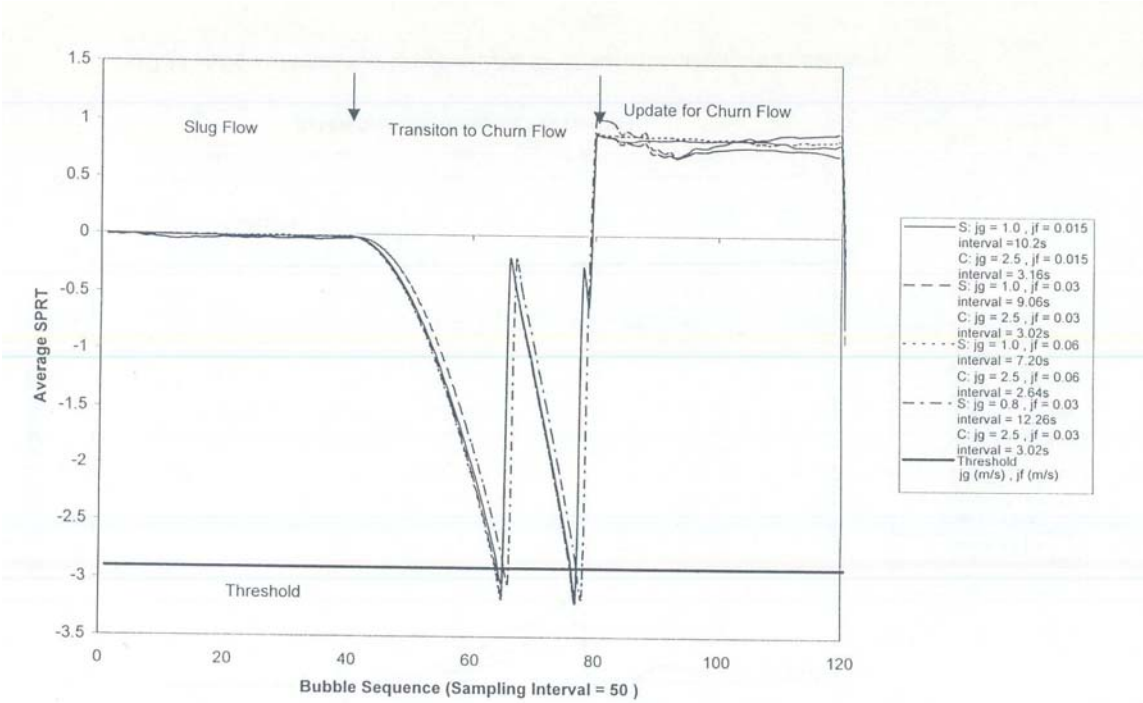

Figure 4.34 Slug and churn flow transition using average SPRT.

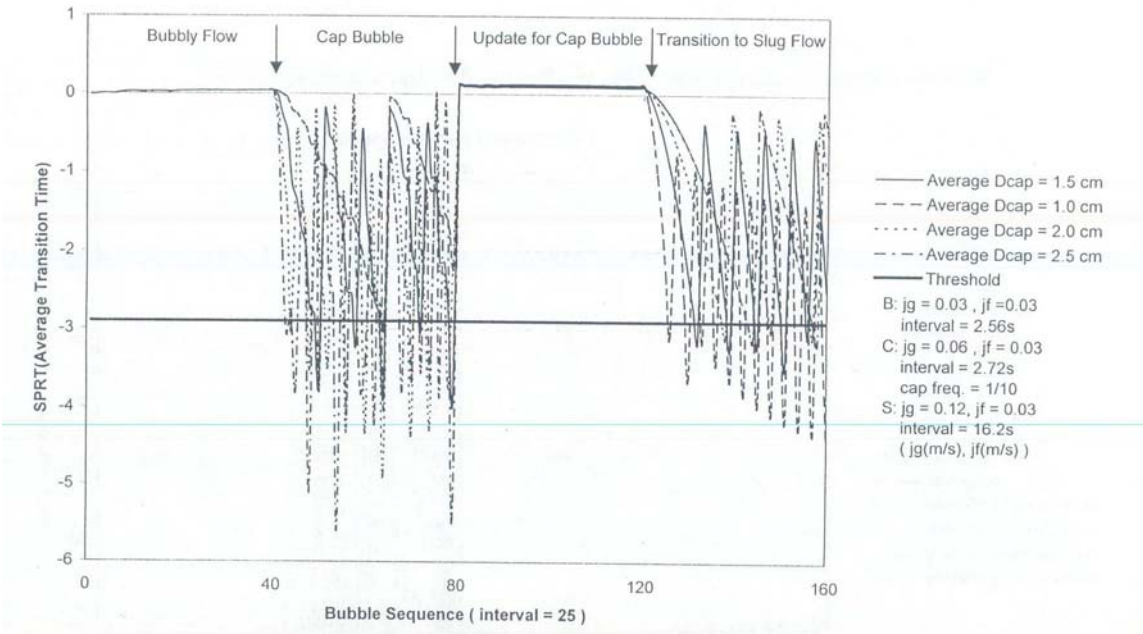

Figure 4.35 Transition between bubbly, cap and slug flow using SPRT based on average transient time for different cap sizes.

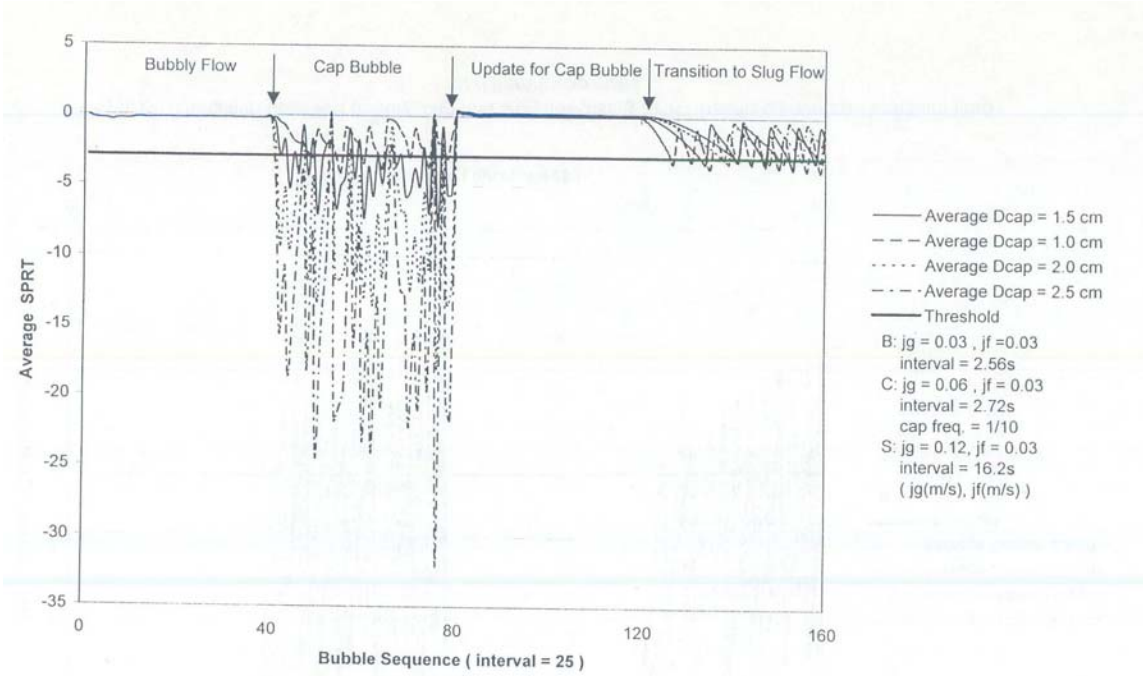

Figure 4.36 Transition between bubbly, cap and slug flow using average SPRT for different cap sizes.

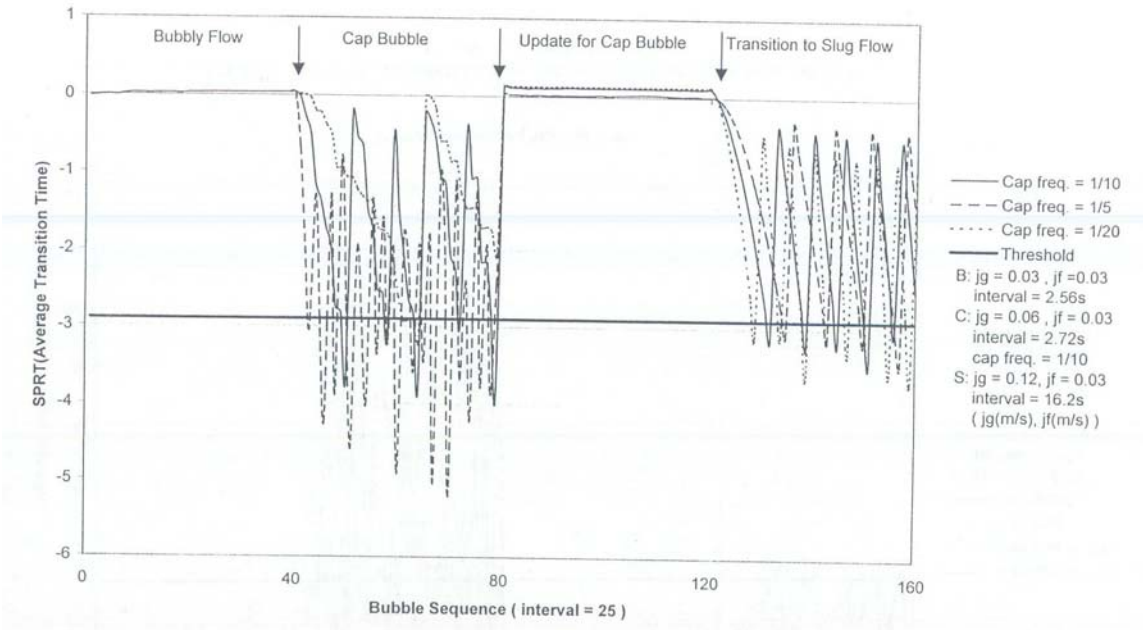

Figure 4.37 Transition between bubbly, cap and slug flow using SPRT based on average transient time for different cap frequencies.

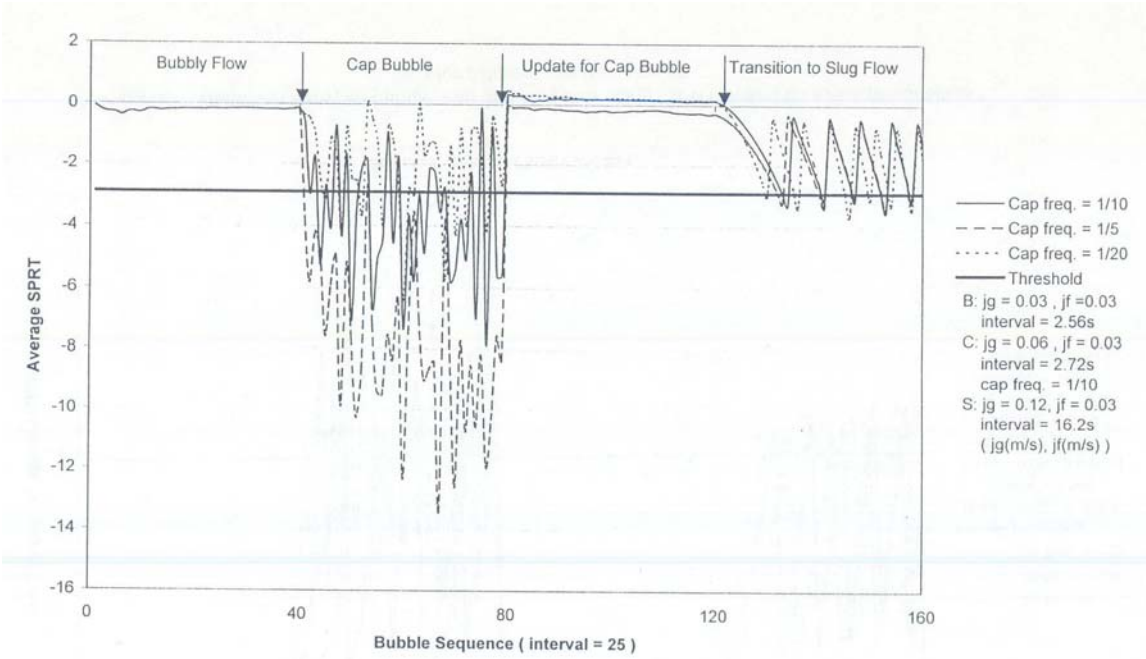

Figure 4.38 Transition between bubbly, cap and slug flow using average SPRT for different cap sizes.

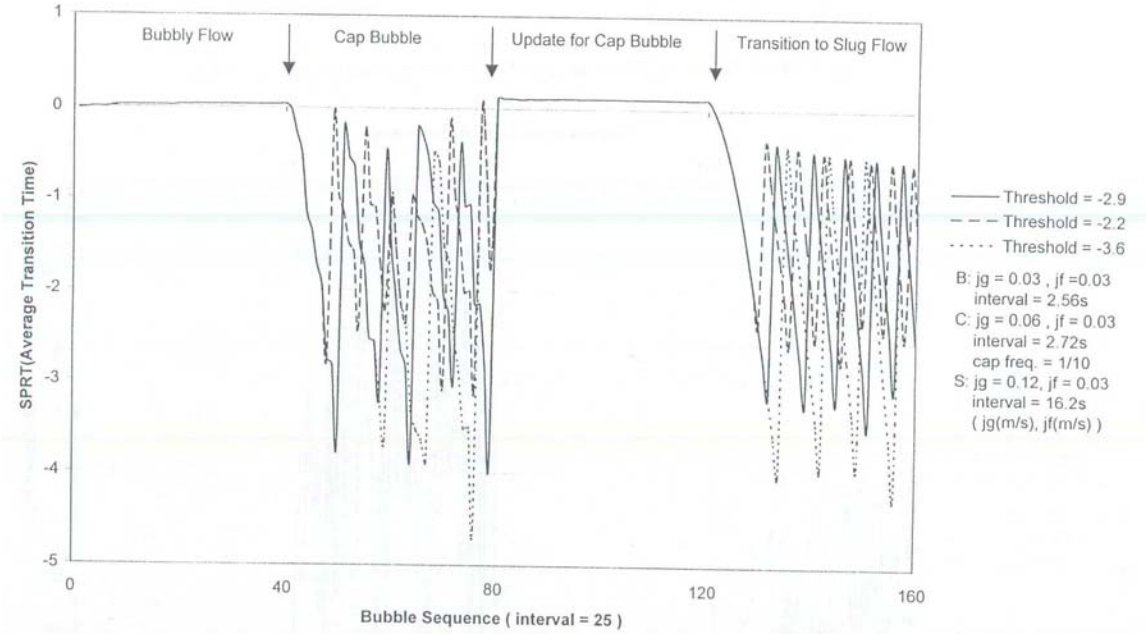

Figure 4.39 Transition between bubbly, cap and slug flow using SPRT based on average transient time for different thresholds.

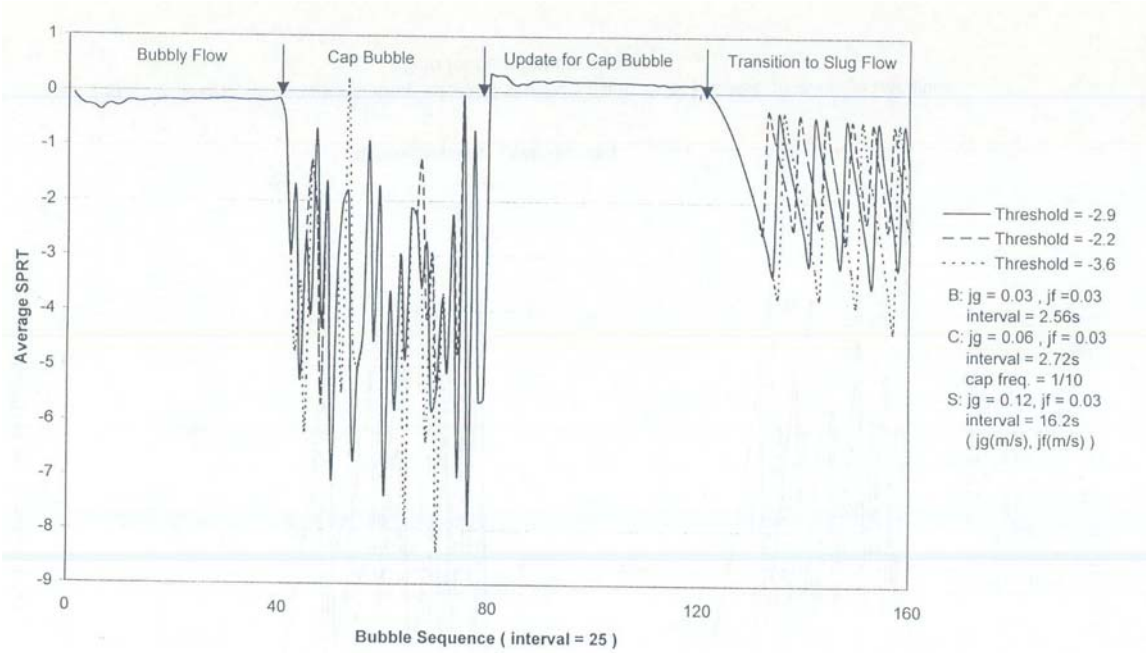

Figure 4.40 Transition between bubbly, cap and slug flow using average SPRT for different thresholds.

4.6. **References**

4.1.M. Ishii, One-Dimensional Drift-Flux Model and Constitutive Equations for Relative Motion between Phases in Various Two-Phase Flow Regimes, ANL-77-47, 1997.

4.2. A. Serizawa, I. Katoka, I. Michiyoshi, Turbulence Structure of Air-Water Bubbly Flow, II. Local Properties, *Int. J. Multiphase Flow,*vol.2, pp. 235-246, 1975.

4.3.P. Griffith, G. B. Wallis, Two-Phase Slug Flow, *Journal of Heat Transfer*, Vol.83, pp.307-320, 1961.

4.4.K. Akagawa, T. Sakaguchi, Fluctuation of Void Ratio in Two-Phase Flow(2nd Report, Analysis of Flow Configuration Considering the Exeistence of Small Bubbles in Liquid Slugs), *Bull. JSME,* Vol. 9, pp 104-110,1966.

4.5. D. Barnea, L. Shemer, Void Fraction Measurements in Vertical Slug Flow: Applications to Slug Characteristics and Transition, *Int. J. Multiphase Flow*, Vol. 15, pp. 495-504, 1989.

4.6. K. Mishima, M. Ishii, Flow Regime Transition Criteria for Upward Two-Phase Flow in Vertical Tubes. *International Journal of Heat and Mass Transfer*, vol. 27, no. 5, pp. 723-737, 1984.

4.7. F. C. Fernandes, R. Semiat, A. E. Dukler, Hydrodynamic Model for Gas-Liquid slug Flow in Vertical Tubes, AICHE, Vol. 25, no.6, pp.981-989,1983.

4.8. Orell, R. Rembrand, A Model for Gas-Liquid Slug Flow in a Vertical Tube, Ind. Eng. Chem. Fundam., Vol. 25,pp. 196-206, 1986.

4.9. Y. Mi, Flow Regime Identification and Vertical Slug Flow Characterization, *Purdue University Ph. D. Thesis*, 1998.

4.10. J. O. Hinze, Fundamentals of the Hydrodynamic Mechanism of Splitting in Dispersion Processes, *AICHE J.*, Vol. 1, pp. 289, 1955

4.11. I. Katoka, M. Ishii, K. Mishima, Generation and Size Distribution of Droplet in Annular Two Phase Flow, *J. Fluids Engineering*, Vol. 105, pp. 230, 1983.

4.12. G.J. Zhang, M. Ishii, Isokinetic Sampling Probe and Image Processing System for Droplet Size Measrement in Two Phase Flow, International Journal of Heat & mass Transfer, Vol. 38, No. 11, pp. 2019-2027, 1995.

4.13. A. Wald, *Sequential Analysis*, John Wiley & Sons, New York, 1947.

4.14. A. Wald and J. Wolfowitz, Optimum Character of the Sequential Probability Ratio Test, *Ann. Math. Stat*, Vol.19, pp 326, 1948.

4.15. K. S. Fu, Sequential Methods in Pattern Recognition and Machine Learning, Academic Press, New York, 1968.

4.16. K. Humenik, K. C. Gross, Using Fourier Series Methods to Reduce Correlation of Nuclear Power Reactor Data, *Nuclear Science & Engineering*, Vol. 112, no. 2, pp. 127-135, 1992.

5. EXPRIMENTAL PROGRAM

The experimental program consists of design of the experimental loop, setting up experimental procedures, performing two phase flow test runs to generate the various flow regimes at various gas and liquid flow rates.

5.1 Experimental Loop

The schematic of the experimental set-up is shown in Figure. The test loop is comprised of test section, separator, water tank, pump, air supply line, various instruments for water and air flow measurement, valves and associated piping.

Test Section

The test section is a 3″ ID acrylic tube which is mounted vertically. Air and water are supplied at the bottom of the test section and they flow vertically upwards. The figure shows the entrance of air and water to the test section.

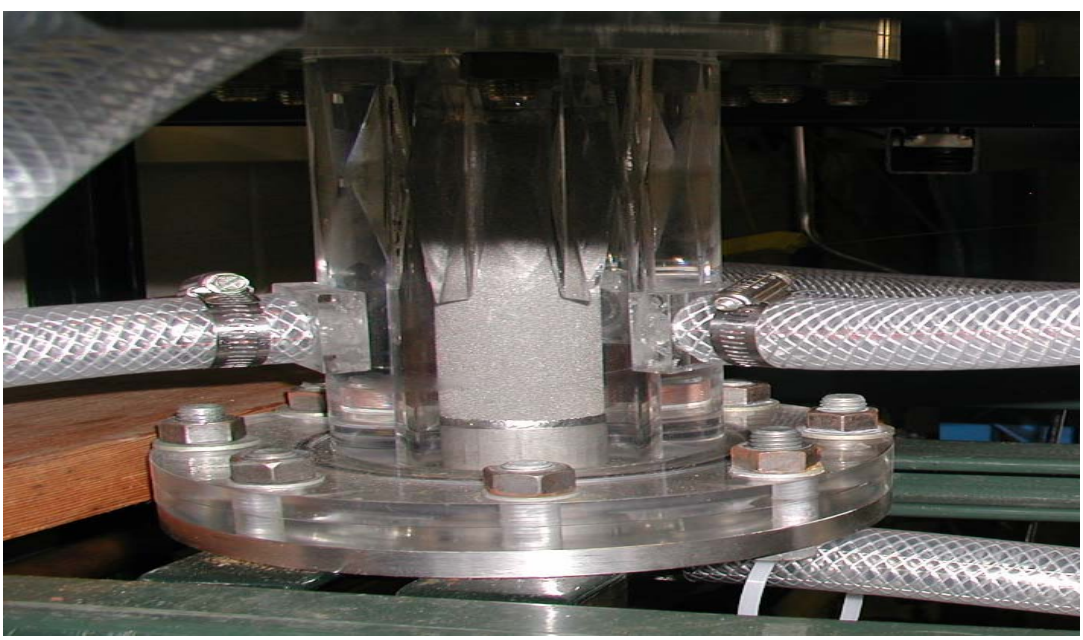

Figure 5.1. Inlet to the test section

The entrance to the test section is constructed in such a way that will result in the proper mixing of water and air at the inlet. Water enters through 4 inlets, three on the side at equal angles from each other and the fourth inlet is at the bottom of the tube. There are baffles constructed on the inside of the tube to prevent eddies or vortex formation at the inlet. There is a porous steel rod inside the tube at the inlet. Air enters at the bottom of the tube through the porous steel rod. This helps in proper atomization of the air at the inlet.

There are 4 taps on the main test section. They are used to hold conductivity probes as well as pressure taps. The first one is approximately 20″ from the bottom. The other probes are placed at a distance of 50″, 80″ and 130″ from this probe. The total height of the test section is approximately 3.8m.

Air Supply Line

Air supply line is connected to the bottom of the test section. Before the connection to steam line, three rotameters with different flow ranges are installed to measure the wide range of air flow rate. A pressure gauge is also installed to measure pressure of air. The air is checked by a valve before entering the test section. The air supply line is a nylon 6 tubing which is 1/8” OD.

Water Tank

The water tank is used for collection of water from the test section. It completes the loop and supplies water to the pump which feeds it back into the loop.

Separator

The separator is drum placed at the top of the test section which is used to collect the water and air after passing through the test section. A baffle is attached to the end of the

test section tube so that the excess spilling of water outside of the separator is avoided. The separator then feeds the water to the water tank and thus completes the loop.

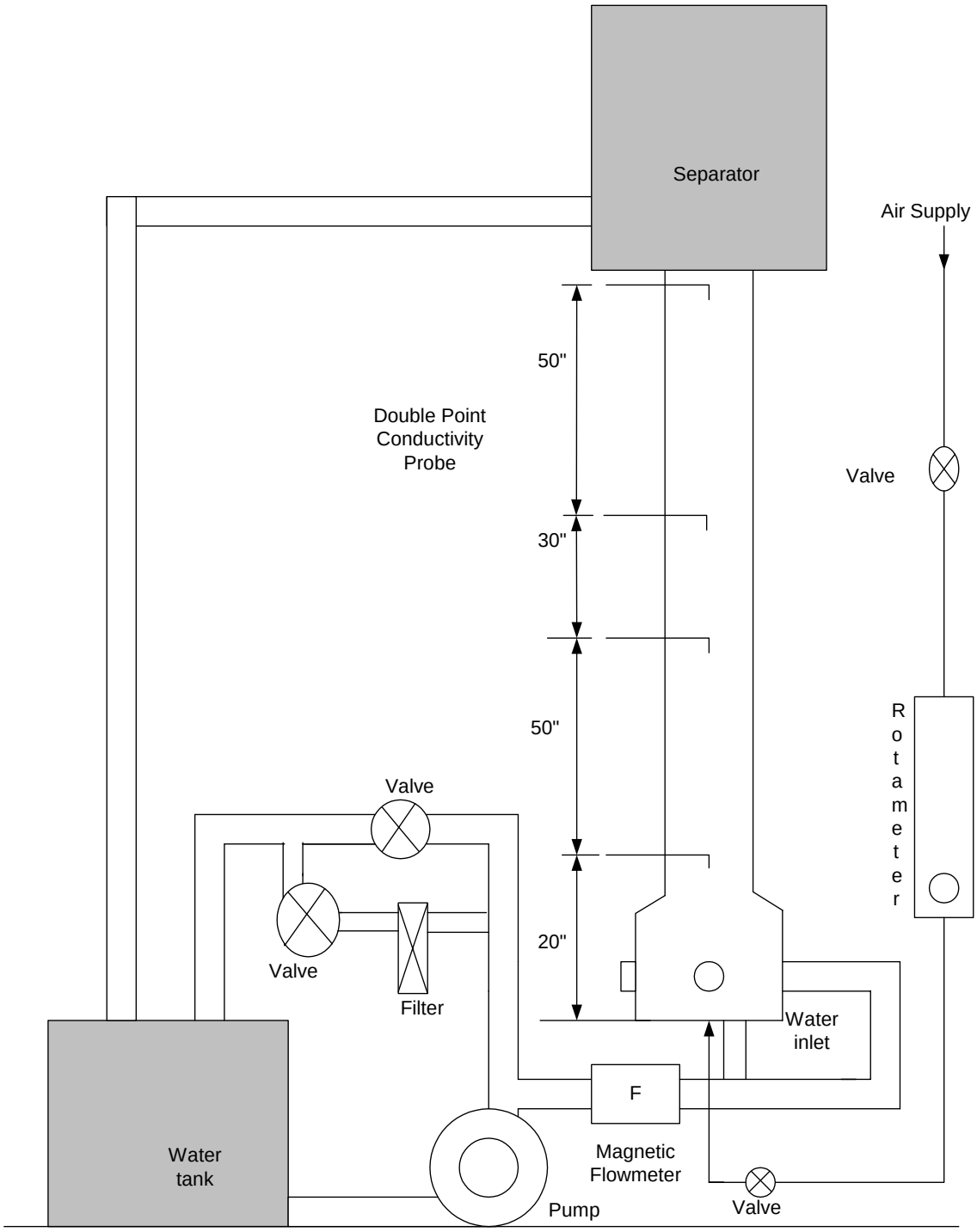

Figure. 5.2. Schematic of the experimental loop.

Water supply line

The water supply line consists of piping and instruments from the pump to the inlet of the test section. There are two water flow lines from the pump to the inlet of the test section. The two pipes are 1" and 1.5" ID. The pipes are connected such that they can be run independently as well as together. This is done to get a wider range of water flow rate. Both the pipes are equipped with magnetic flow meters to measure the liquid flow rate. An air filter is installed in the water supply line to clear out any impurities in the water.

Table 5.1 List of Instruments

Variable	Process	Instrument	Tag. No.
Flow Rate	Water	Magnetic Flow Meter	FT1, FT2
	Air	Rotameter	FA1, FA2, FA3
Pressure	Water (test section)	Pressure Gauge	DP1
	Air Supply line	Pressure Gauge	PG1

Description of Instruments

Pressure

DP1: Test Section DP
PG1: Pressure gauge to measure the air inlet flow pressure.

Flow

FT1: Magnetic flow meter for water flow measurement
FT2: Magnetic flow meter for water flow measurement
FA1: Rotameter for air flow rate measurement (high flow)
FA2: Rotameter for air flow rate measurement (medium flow)
FA3: Rotameter for air flow rate measurement (low flow)

Description of Valves

Valve type and normal position (NO-normal open, NC-normal closed) are shown in parenthesis.

Water Line

VW1: Water flow control valve on the water inlet pipe (1.5" Dia) (Needle, NC)
VW2: Water flow control valve on the water inlet pipe (1" Dia) (Needle, NC)
VW3: Water flow control valve to the pump from the water tank (Needle, NO)
VW4: Water flow control valve to the filter from the pump (Ball, NO)
VW5: Water flow control valve to the test section inlet from the pump (Ball, NO)

Air Supply Line

VA1: Air supply line valve (ball, NO)
VA2: Air supply line valve upstream flowmeter (ball, NC)
VA3: Air supply line valve just before test section (ball, NC)

5.2 Experimental Data

As stated earlier, there are 4 probes in the experimental loop. The data from the four probes is then converted into digital signals and directly recorded in a computer with the help of a data acquisition board. In this experiment, Keithley's DAS-1801ST is used with a STA 1800U accessory. The DAS board is capable of simultaneously obtaining data from as many as 16 single inputs or 8 differential measurements. In our loop, data is taken for 8 single inputs. The probes have two signals coming out corresponding to each probe tip. Each measurement is then coupled with ground to give us the corresponding signal. Since only the transition time (i.e. time for the bubble flow) is of interest, data is obtained from only one probe tip. (Data from both the probe tips are needed for the measurement of bubble superficial velocity.)

The data coming from the probes is first passed through a comparator circuit before feeding it to the computer. The comparator circuit corrects the data for noise and also rectifies the data so that the probe signals are close to the ideal simulated signals in appearance. This offers the advantage of directly using the experimental data for the calculation of void fraction, signal time traces and PDFs.

A quad-Amp is used to process the signal from each of the probe simultaneously. The schematic shown in Fig. 5.3 is for one single amp. A 9V DC source is used for the signal input. Output from the circuit is in the range of 0-5V DC. Also there is the option of setting the threshold value for the measurement of output data, so that the cut off level to eliminate the noise can be set by the user.

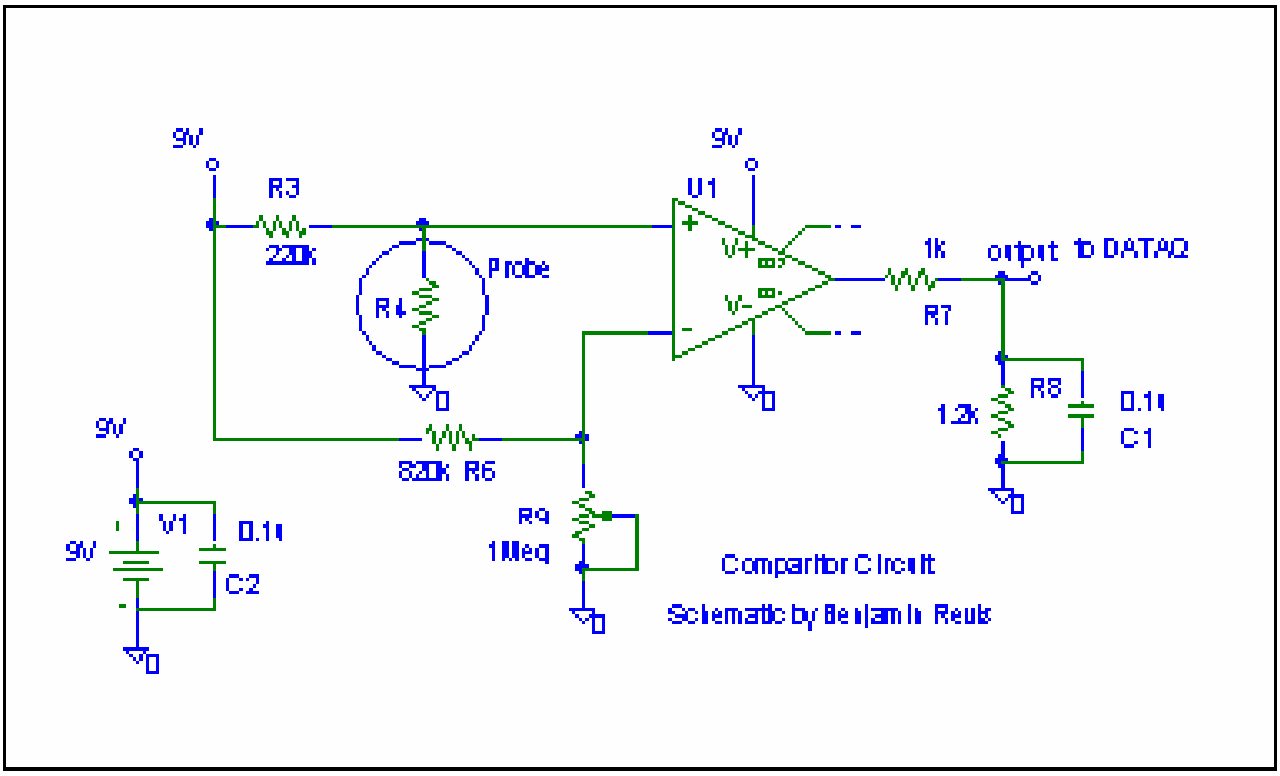

Figure 5.3 Schematic of the comparator Circuit.

At present, detailed experiments have not been carried out to obtain data from the experimental loop for all flow regimes. Here, a sample data acquisition is presented in the bubbly flow regime corresponding to a liquid flow rate of 2.1 GPM and a gas flow rate of 10 SCFM.

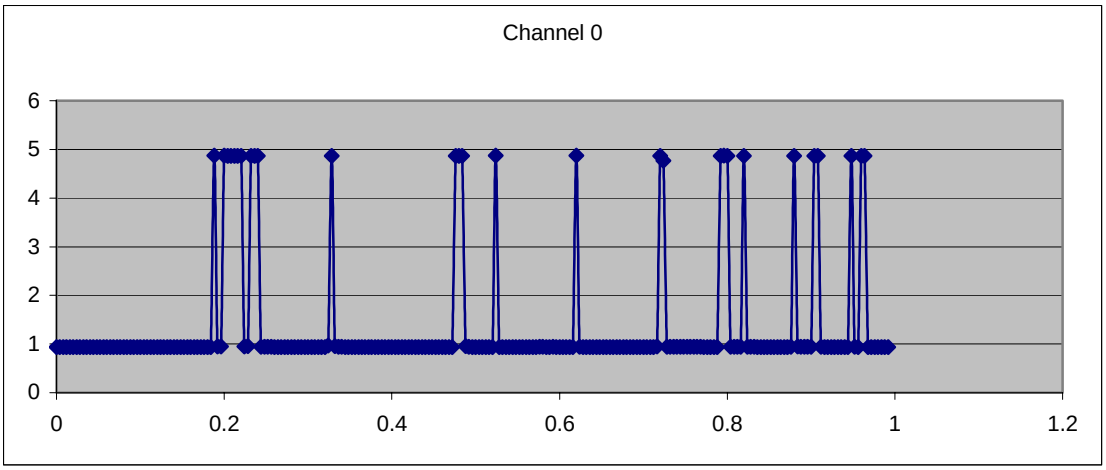

Figure 5.4 Sample output from the data acquisition system.

6. PROTREN RESULTS

PROTREN is a program which uses fuzzy logic methodology to detect the onset of transients. Recently work has been done to improve the performance of PROTREN to include artificial neural networks. In the current research, the older version of PROTREN has been tested on sample data obtained from the Monte-Carlo Simulation to show indicative results as well as the shortcomings of this version.

Currently, PROTREN does not have the capacity of working with the data in real time. The data has to be processed, i.e. the data has to be normalized so that its mean is 1 and the standard deviation is 1.

In the following figs, a combination of two bubble sizes (4mm dia. and 8mm dia.) is used to show a change in void fraction. Depending on the change in void fraction, it is expected to find a change in PROTREN indicating a transient.

In Fig. 6.1 and 6.2, PROTREN is tested for a signal in which an increase in bubble diameter takes place for a short time. As is seen, PROTREN detects this change pretty accurately.

In Fig 6.3 and 6.4, PROTREN is tested for a data in which the bubble diameter is 8mm to begin with. It dips down to 4mm , which is followed by a short period of time in which the bubble diameter is 8 mm and then followed by 4mm dia bubbles. As is seen, PROTREN is unable to detect any transients in this process. This is currently one of the major shortcomings of PROTREN, i.e. it cannot detect multiple transients in a process.

Figs. 6.5 and 6.6 show the results for a decreasing transient. This can be detected by PROTREN, but as can be seen, the detection is not accurate.

These shortcomings of PROTREN will be addressed in future research work.

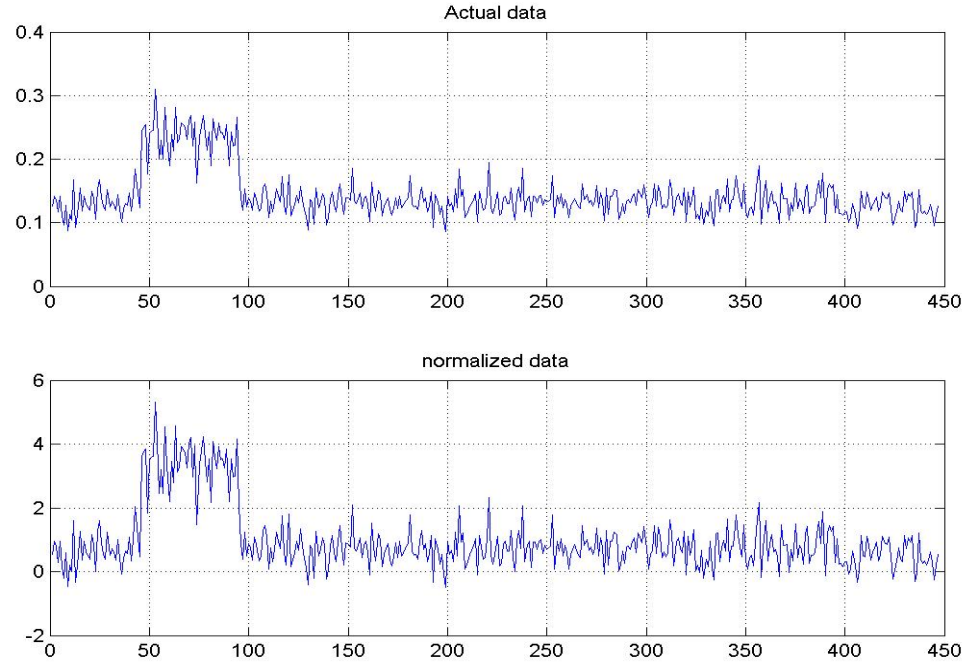

Figure 6.1 actual data and normalized data for an increasing transient.

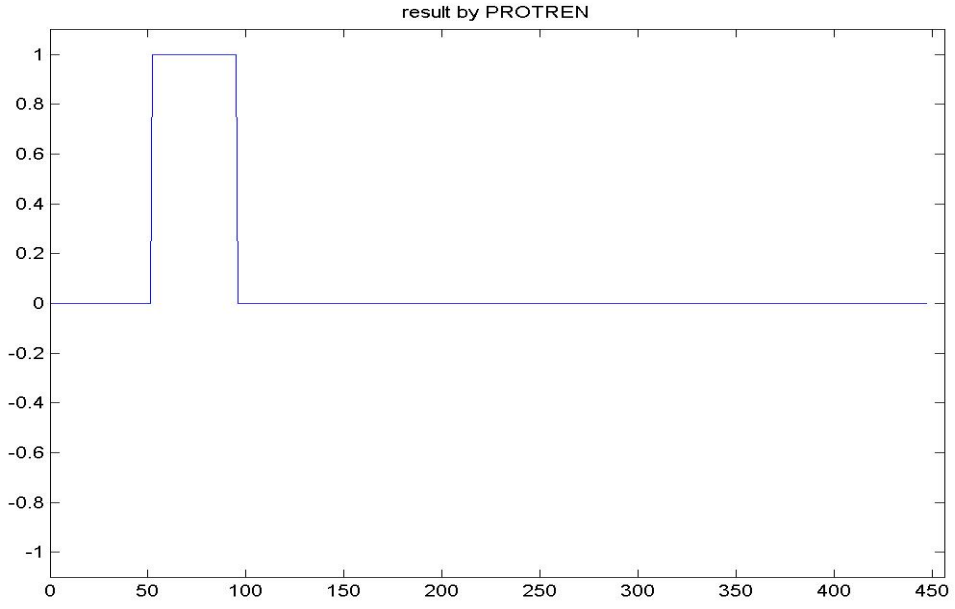

Figure. 6.2 PROTREN result for an increasing transient.

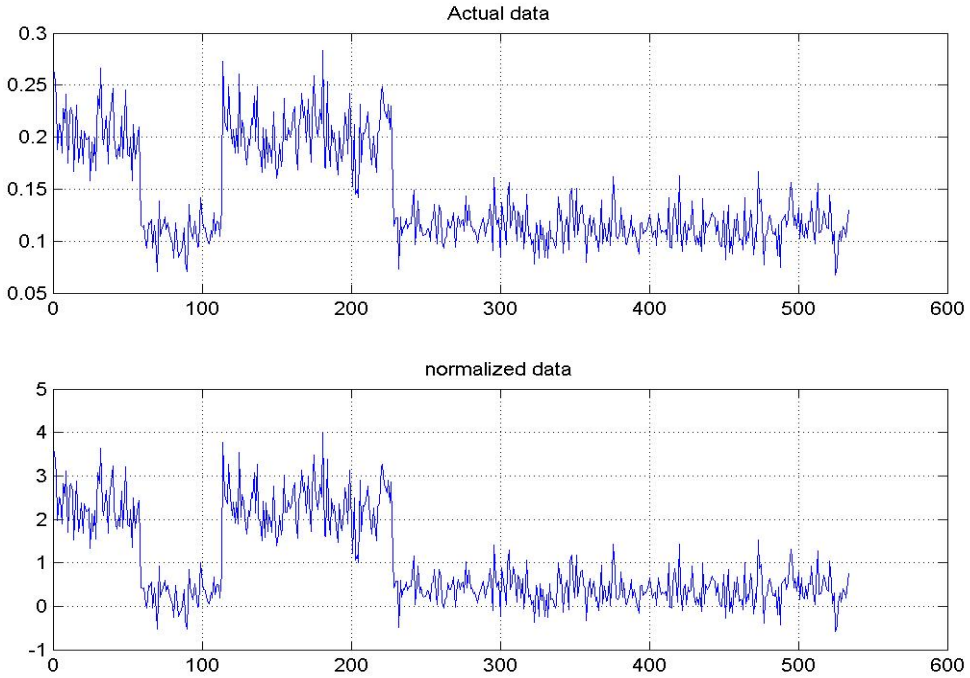

Figure 6.3 Actual and Normalized data for fluctuating transient

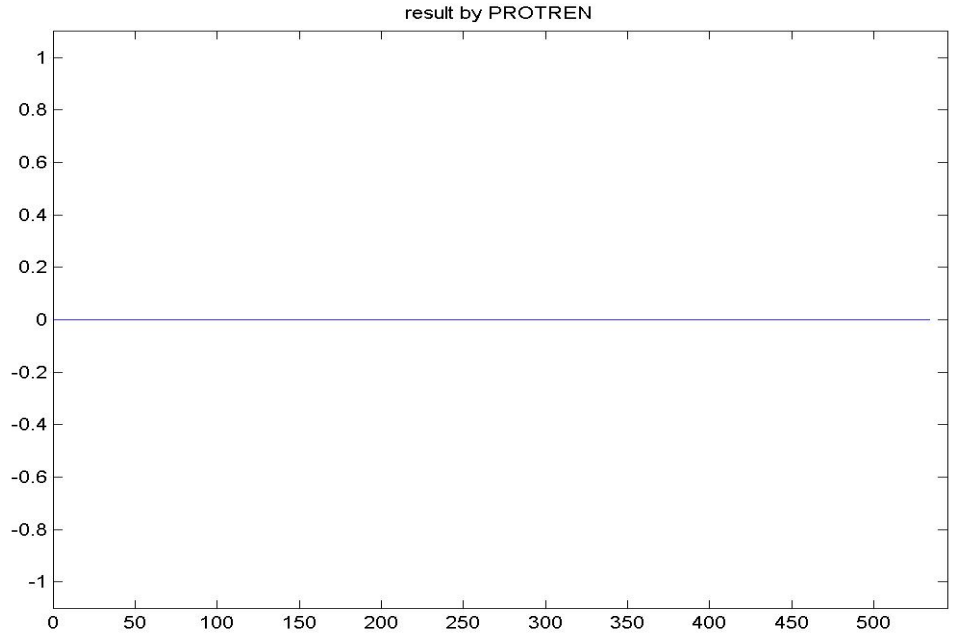

Figure. 6.4 PROTREN result for a fluctuating transient.

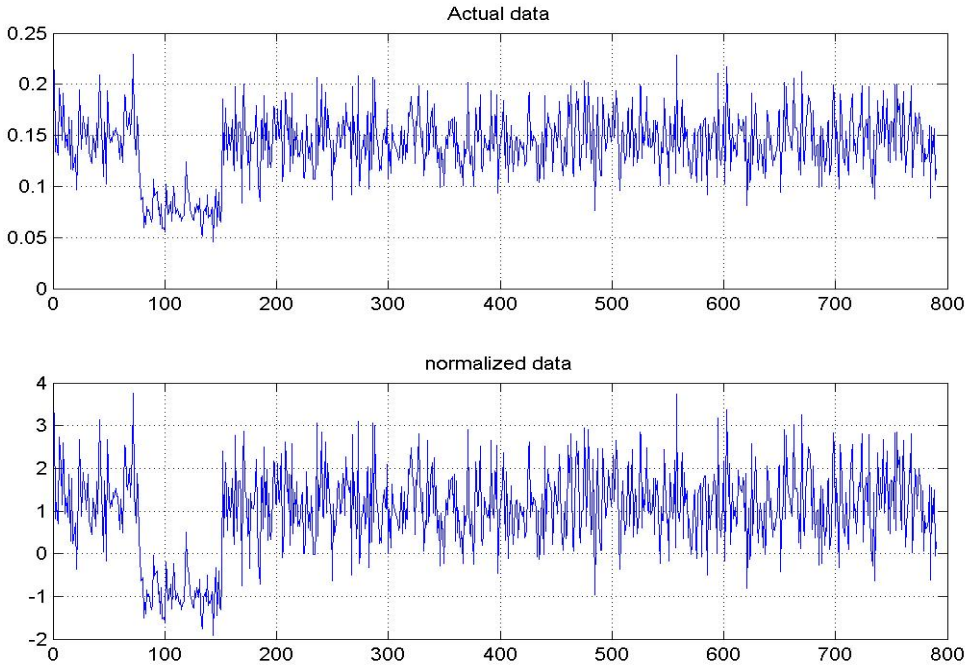

Figure 6.5 Actual and normalized data for a decreasing transient

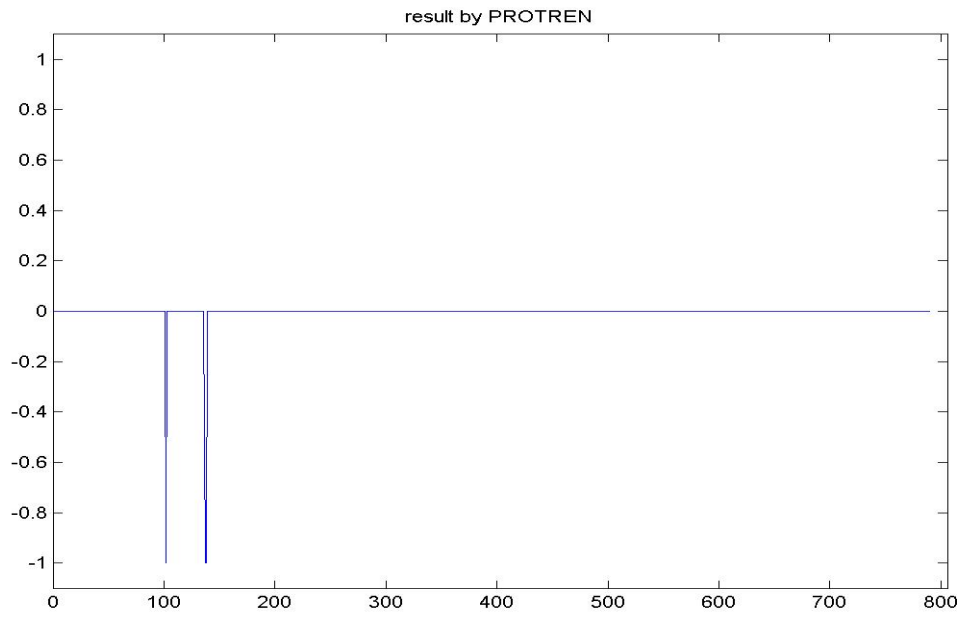

Figure 6.6PROTREN result for a decreasing transient.

7. SUMMARY OF THE FIRST YEAR WORK

The following are the accomplishments for the first year of research:

1. The work on the experimental loop has been completed. The instrument panel has been installed. Also there are four probes set up on the experimental loop. Work has also been finished on the data acquisition system and the loop is now ready to take data.
2. Monte Carlo simulation has been carried out to simulate the various phases of the two phase flow of water and air through a vertical channel. This simulation gives the flow regimes for the various phases of the two phase flow. These results are then used to test PROTREN for correct prediction of change in phase.
3. An alternative methodology, SPRT (Sequential Probability Ratio Test) was developed. SPRT is used to detect the changes in flow rate when the phase changes from one phase to another. The results from SPRT are used to compare the results from PROTREN so that the results from PROTREN can be verified. Also, SPRT helps in making improvements in the current version of PROTREN.

8. FUTURE WORK

The future work will involve the following main areas of research:

1. Work will be carried out to make improvements in the current version on PROTREN. The goal will be to make PROTREN capable of detecting transients online. Also PROTREN will have more features such as the ability to detect multiple transients, inclusion of other transient detection methods like SPRT etc.
2. The loop is now ready for data acquisition. Data will be taken for different flow regimes. This data will be used to run and verify PROTREN.
3. Data from the condensation loop will be used to benchmark and validate PROTREN.
4. PROTREN will be used to run the data from the nuclear reactor neutron flux data. The nuclear reactor data and the data from a scaled advanced boiling water reactor system will be used to develop an integral system testing of PROTREN.